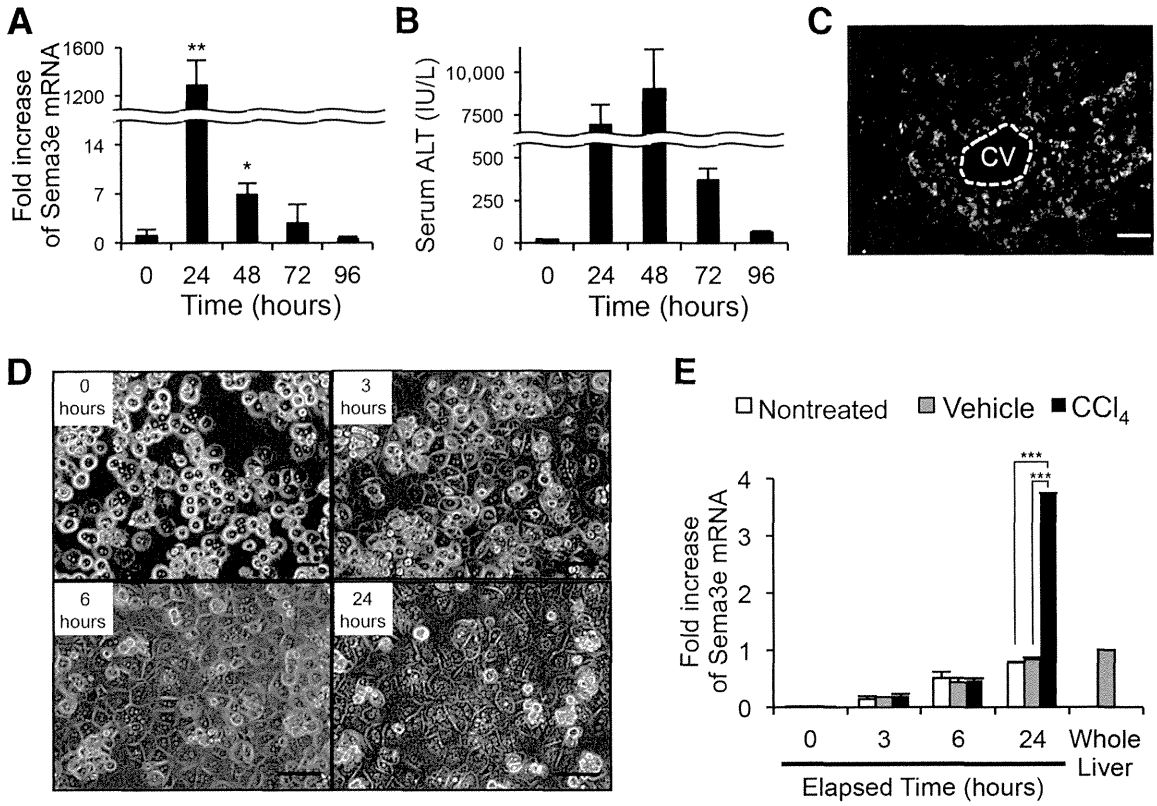


**Figure 2** Expression profiles of semaphorin 3E (Sema3e) and plexin D1 (Plxnd1) in liver. **A:** Sema3e expression level in liver after carbon tetrachloride ($CCl_4$)—induced injury. **B:** Whole liver total RNA was assessed by quantitative RT-PCR. Evaluation of serum alanine aminotransferase level at indicated time points. **C:** Livers were subjected to immunohistochemical staining with an anti-Sema3e antibody 24 hours after $CCl_4$ treatment. Sema3e expression is observed in hepatocytes in the damaged region around the central vein. **D:** Morphologic alterations in primary cultured hepatocytes treated with $CCl_4$. **E:** The expression levels for *Sema3e* of primary cultured hepatocytes at 0, 3, 6, and 24 hours after nontreatment, vehicle treatment, or $CCl_4$ treatment, respectively. The whole liver represents the mRNA of injured mouse liver 24 hours after $CCl_4$ administration. The fold expression of Sema3e mRNA of cultured hepatocytes relative to the whole liver is shown. Data are expressed as means ± SEM. $n = 3$ per group. $^*P < 0.05$, $^{**}P < 0.01$, and $^{***}P < 0.001$ versus 0 hours after $CCl_4$ treatment. Scale bars: 50 μm (**C**); 100 μm (**D**).

Sema3e (Supplemental Figure S2A). Moreover, Sema3e was not induced after a 70% partial hepatectomy, which was not accompanied by hepatocyte damage (Supplemental Figure S2B). These results strongly suggest that Sema3e is induced in hepatocytes *in vitro* and *in vivo* in a damage-dependent manner.

## Sema3e Has an Effect on Retracting SEC Filopodia

We isolated each type of liver cell by fluorescence-activated cell sorting and analyzed Sema3e receptor (Plxnd1) expression by RT-qPCR to identify the cell type that responded to Sema3e in injured liver. Plxnd1 was predominantly expressed in Stab-2$^+$ SECs (Figure 3A), suggesting that Sema3e secreted from degenerating hepatocytes could affect SECs in a paracrine fashion. Sema3e plays a role in repulsing the endothelial tip and inhibiting cell migration. However, the effect of Sema3e on SECs has not been examined. Therefore, we investigated the effect of Sema3e on freshly isolated SECs in culture. As a result, SEC filopodia retracted significantly in the presence of Sema3e (Figure 3, B and C), as reported previously in other endothelial cell lines.[18,27]

## Prolonged Expression of Sema3e Results in Disoriented Sinusoidal Regeneration

Given that Sema3e also induced retraction of SEC filopodia *in vivo*, transient expression of Sema3e from damaged hepatocytes could be involved in the morphologic contraction of SECs as observed 24 hours after $CCl_4$ treatment (Figure 1D and Supplemental Figure S1D). This idea was supported by the result that SECs returned to their original morphologic status during reconstruction of sinusoids after the drastic decrease in Sema3e expression. To further verify Sema3e function *in vivo*, we examined the effect of prolonged Sema3e expression by HTVi, which is a method of delivering an expression vector into hepatocytes. We initially injected either Sema3e or a control expression vector into wild-type mice by HTVi. Then, each mouse was treated with either $CCl_4$ or vehicle 3 days after HTVi. We first examined SEC by using H&E and IHC staining 1 day after $CCl_4$ administration when endogenous Sema3e expression is drastically induced. We observed no obvious differences in the damaged area between control- and Sema3e-HTVi liver (Supplemental Figure S3). These results

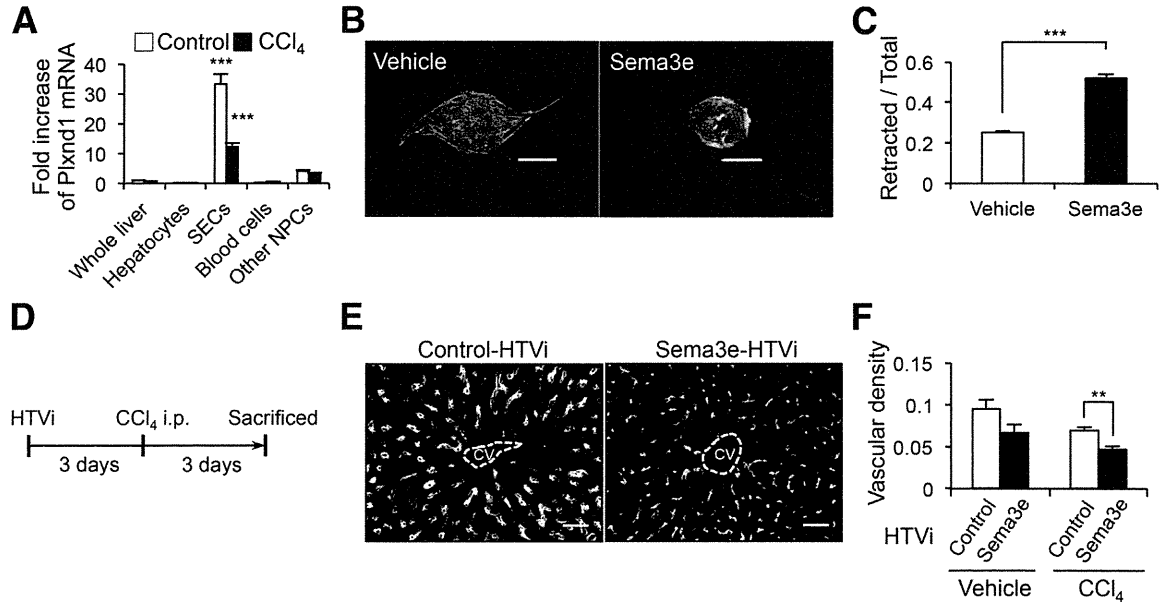


**Figure 3** Semaphorin 3E (Sema3e) induces contraction of sinusoidal endothelial cells (SECs). **A:** Real-time RT-PCR analysis of plexin D1 (Plxnd1) in hepatocytes, SECs, blood cells, and other non-parenchymal cells (NPCs). Each fraction was isolated from normal or 24-hour post—carbon tetrachloride ($CCl_4$) liver, and Plxnd1 mRNA levels were compared with those of whole livers. Remarkable Plxnd1 expression was observed in SECs in normal and 24-hour post-$CCl_4$ livers. **B:** Morphologic changes in SECs after addition of Sema3e. **C:** SECs were subjected to primary culture with or without Sema3e. SECs cultured with Sema3e have significant retraction of filopodia observed in control SECs. **D:** Scheme of *in vivo* analysis using the hydrodynamic tail-vein injection (HTVi) method. **E:** The Sema3e expression vector was introduced into hepatocytes using the HTVi method. The mice were subjected to $CCl_4$ injection after 3 days. Then, livers were harvested after an additional 3 days. Immunostaining of liver sections with an anti—stabilin (Stab)-2 antibody 3 days after injury. **F:** Normal sinusoidal regeneration is observed in the control liver, whereas disorganized regeneration of contracted SECs is observed in Sema3e-expressed livers. Vascular density of control- and Sema3e-expressed liver sections before and after injury. The SEC area significantly decreases in Sema3e-expressed livers after liver injury. Vascular area was measured as Stab-2—positive area visualized by immunohistochemistry. Empty areas, such as the lumen, were subtracted for calculation. Data are expressed as means ± SEM. $n = 3$ per group (**A**); $n = 4$ per group (**C**); $n = 4$ to 5 per group (**F**). $^{**}P < 0.01$, $^{***}P < 0.001$ for analysis of variance with Tukey's post hoc tests. Scale bars: 20 μm (**D**); 50 μm (**F**).

suggested that the additional overexpression of Sema3e was not effective because the amount of endogenous Sema3e was enough to affect sinusoidal contraction 1 day after liver injury. Then, we analyzed the livers 3 days after $CCl_4$ administration when endogenous Sema3e expression is decreased (Figure 3D). Sinusoidal regeneration and SEC status were evaluated by IHC using an anti—Stab-2 antibody and vascular density, as represented by the ratio of the Stab-2—positive area to total parenchymal area (Figure 3, E and F). We confirmed that exogenous Sema3e expression by HTVi was maintained irrespective of $CCl_4$ treatment (Supplemental Figure S4). Although the vascular system of Sema3e-HTVi livers tended to decrease compared with that of control-HTVi livers, no significant difference was observed in vehicle treatment (Figure 3F). The Sema3e-HTVi liver treated with $CCl_4$ had markedly disoriented and contracted SECs, whereas radial arrays of SECs were reconstructed around the CV in control-HTVi liver (Figure 3E), which was similar to the image 24 hours after $CCl_4$ treatment (Figure 1D and Supplemental Figure S1D). Consistent with this observation, the vascular system of the Sema3e-HTVi liver decreased significantly compared with that of the control-HTVi liver (Figure 3F). These results suggest that Sema3e is able to affect the morphologic status of SECs in regeneration process *in vivo* and *in vitro*.

## Disoriented Sinusoidal Regeneration by Sema3e Potentiates HSC Activation *in Vivo*

We examined whether regeneration of hepatocytes was affected after liver injury because inhibiting sinusoidal reconstruction in Sema3e-HTVi liver may affect blood flow in the liver. However, no significant differences were observed between control- and Sema3e-HTVi livers after H&E staining (Figure 4A) or by serum albumin concentration (Supplemental Figure S5). We next investigated the status of HSCs, another key component of the liver sinusoid. Because HSCs express p75 low-affinity neurotrophic growth factor receptor (p75NTR),[28,29] SECs and HSCs in a regenerating sinusoid were visualized by IHC using anti—Stab-2 and anti-p75NTR antibodies. Normal sinusoids were reconstructed in control-HTVi liver 3 days after $CCl_4$ treatment (ie, each HSC-lined SEC was rearranged correctly). In contrast, many extended HSCs were observed accompanied by disorganized revascularization in the Sema3e-HTVi liver (Figure 4B). Moreover, most of these HSCs were not lined by SECs. HSCs and SECs are reciprocally regulated, and transient activation of HSCs is beneficial for wound healing during regeneration. Therefore, we supposed that the activation of HSCs was prolonged because of the lack of regulation by SECs. Actually, an expression analysis of α-smooth

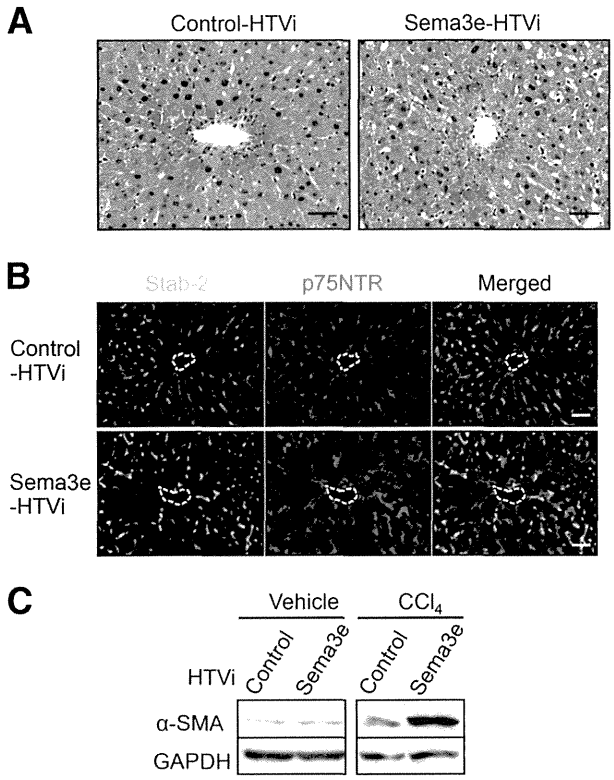


**Figure 4** Disoriented sinusoidal regeneration by semaphorin 3E (Sema3e) potentiates hepatic stellate cell (HSC) activation *in vivo*. **A:** Hematoxylin and eosin staining of liver sections 3 days after carbon tetrachloride ($CCl_4$) treatment. No apparent difference is observed between control—hydrodynamic tail-vein injection (HTVi) and Sema3e-HTVi livers. **B:** Immunostaining of liver sections with anti—stabilin-2 (Stab-2) and anti-p75 low-affinity neurotrophic growth factor receptor (p75NTR) antibodies 3 days after $CCl_4$ treatment. Many HSCs in Sema3e-HTVi liver are not lined by sinusoidal endothelial cells (SECs) compared with that in control-HTVi liver. Broken line indicates central vein. **C:** Western blot analysis of α-smooth muscle actin (α-SMA) in liver 3 days after treatment with vehicle or $CCl_4$. α-SMA protein level in $CCl_4$-treated liver increases markedly in Sema3e-HTVi liver compared with the control, whereas the levels in vehicle-injected livers are not significantly different between Sema3e-HTVi and control-HTVi liver. Scale bar = 50 μm. GAPDH, glyceraldehyde-3-phosphate dehydrogenase.

muscle actin, an HSC activation marker, by Western blot analysis revealed activation of HSCs in Sema3e-HTVi liver compared with that in control-HTVi liver (Figure 4C). In contrast, the vehicle treatment did not activate the HSCs irrespective of continuous Sema3e expression, suggesting that Sema3e does not directly activate uninjured HSCs. Thus, Sema3e is likely to activate HSCs through SECs only when the sinusoid is undergoing reconstruction. These results suggest that transient expression of Sema3e by degenerating hepatocytes might contribute to the initial step of wound healing by activating HSCs.

## Consecutive Expression of Sema3e Is a Risk Factor for Liver Fibrosis

Hepatocytes continue to be damaged in chronic hepatitis, and sinusoids are regenerated repeatedly. Given that continuous Sema3e expression resulted in activating HSCs, consecutive exposure of Sema3e under chronic hepatitis might contribute to the risk of fibrosis through prolonged HSC activation. We used *Sema3e*-KO mice to address this hypothesis. First, we compared hepatocellular damage induced by a single administration of $CCl_4$ between wild-type and *Sema3e*-KO mice. We found no significant difference in serum ALT level between both genotypes after $CCl_4$ administration (Supplemental Figure S6), suggesting that Sema3e deficiency does not directly affect the $CCl_4$-mediated hepatocellular cytotoxicity. Second, we evaluated the morphologic status of SECs and HSCs 24 hours after

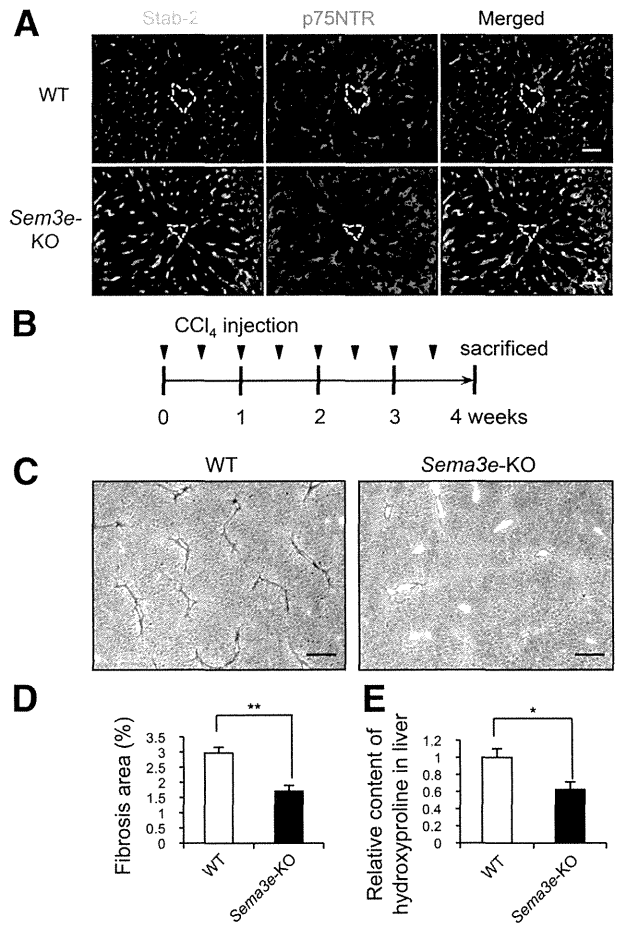


**Figure 5** Lack of semaphorin 3E (Sema3e) affects sinusoidal regeneration and attenuates liver fibrosis. **A:** Immunostaining of liver sections with anti—stabilin-2 (Stab-2) and anti-p75 low-affinity neurotrophic growth factor receptor (p75NTR) antibodies 24 hours after carbon tetrachloride ($CCl_4$) treatment. **B:** Sinusoidal endothelial cell (SEC) morphologic status in wild-type (WT) mice is markedly contracted, whereas that of *Sema3e*-knockout (KO) mice is less affected. Broken line indicates central vein (CV). Experimental scheme for liver fibrogenesis in wild-type and *Sema3e*-KO mice. **C** and **D:** A total of 1.0 mL/kg of i.p. $CCl_4$ was injected into each mouse twice per week for 4 weeks, and then the liver was harvested. Sirius Red staining of liver sections after $CCl_4$ treatment. **E:** WT mouse liver exhibits marked accumulation of fibers around the CV, whereas the *Sema3e*-KO mouse liver appears less fibrotic. Relative hydroxyproline (Hp) content in liver. *Sema3e*-KO livers contain less Hp than WT livers. Data are expressed means ± SEM. $n = 5$ per group. $^*P < 0.05$, $^{**}P < 0.01$. Scale bars: 50 μm (**B**); 200 μm (**E**).

$CCl_4$ treatment in wild-type and *Sema3e*-KO mice. The SECs were markedly contracted in wild-type mice, whereas they were less affected in *Sema3e*-KO mice (Figure 5A). These results indicate that not only the robust expression of Sema3e but also the lack of Sema3e could affect sinusoidal regeneration. Moreover, almost all HSCs were associated with SECs in *Sema3e*-KO mice, but many HSCs were not lined by SECs in wild-type mice (Figure 5A). Finally, the morphologic features of both wild-type and *Sema3e*-KO SECs reverted to the original shape 72 hours after $CCl_4$ treatment (Supplemental Figure S7).

To further investigate the involvement of Sema3e in liver regeneration and fibrosis, chronic hepatitis was induced in wild-type and *Sema3e*-KO mice by repeated administration of $CCl_4$ (Figure 5B). We investigated the proliferation of hepatocytes 72 hours after the final $CCl_4$ injection by IHC using an anti–Ki-67 antibody. We found no significant differences in the rate of Ki-67–positive hepatocytes around the CV between wild-type and *Sema3e*-KO mice (Supplemental Figure S8, A and B). However, Picro Sirius Red staining revealed that the accumulation of collagen fibers was markedly decreased in *Sema3e*-KO mice compared with wild-type mice (Figure 5, C and D). Actually, the hydroxyproline content in liver, which reflects the amount of collagen, decreased significantly in *Sema3e*-KO mice compared with wild-type mice (Figure 5E), indicating that the lack of Sema3e attenuates liver fibrosis. In addition, *Sema3e*-KO SECs around the CV exhibited a more extended morphologic status than wild-type SECs even after chronic injury (Supplemental Figure S9). These results indicate that continuous exposure to Sema3e under a chronic hepatitis condition contributes to the exacerbation of liver fibrosis.

## Discussion

We found that Sema3e plays significant roles in sinusoidal regeneration and the progression of liver fibrosis (Figure 6). We found that damaged hepatocytes transiently expressed Sema3e, which induced contraction of SECs in $CCl_4$-mediated liver injury model. Because free radical derived from $CCl_4$ metabolite damages the liver cells, we cannot exclude the possibility that cytotoxicity or cellular alterations due to proteolysis may partly contribute to the thinner staining of SECs by IHC. However, the staining patterns by two distinct SEC surface markers, Stab-2 and FcγR, exhibited a similar contracted morphologic status. In addition, *Sema3e*-KO SECs were less contracted than wild-type SECs after $CCl_4$ administration despite no significant differences in hepatocellular cytotoxicity, strongly suggesting that contraction of SEC was caused by Sema3e actively rather than passive cellular alterations.

Various functions of semaphorins and their receptors have been revealed recently. Among them, regulation of angiogenesis as a repulsive cue is a well-known function of type 3 semaphorins. In particular, Sema3e inhibits extension of endothelial tip cells that play a significant role in angiogenic guidance. In contrast, Sema3e and Plxnd1 are expressed in macrophages of advanced atherosclerotic plaques and regulate their retention.[26] However, the functional significance of Sema3e in liver disease remains unknown. Because Sema3e and Plxnd1 mRNA were not detected in CD45-positive blood cells, including macrophages in either normal or $CCl_4$-treated liver, it is unlikely that blood cells are related to a series of SEC morphologic changes directly. Meanwhile, Sema3e expression was induced in damaged hepatocytes. Although the signaling pathway implicated in Sema3e expression is largely unknown, Moriya et al[30] found that p53 expression up-regulated Sema3e expression in HUVEC and ischemic limb. Considering that reactive oxygen species (ROS) relate to the activation of p53 signaling,[31] drastic expression of Sema3e in $CCl_4$-injured liver may be promoted in a p53-dependent manner. In addition, the modest induction of Sema3e in primary cultured hepatocytes without ROS suggests the possibility that a cellular stress by dissociation or culture is involved in Sema3e expression. In fact, we have observed that the other hepatitis models, such as concanavalin-A injection or 3,5-diethoxycarbonyl-1,4-dihydrocollidine feeding, also induce potent expression of Sema3e (data not shown), suggesting the existence of another pathway independent of ROS stimuli. Further studies are needed to elucidate alternative signaling pathways.

Secreted type 3 semaphorins have been considered to function in an autocrine manner during angiogenesis. However, our findings indicate that Sema3e may play a

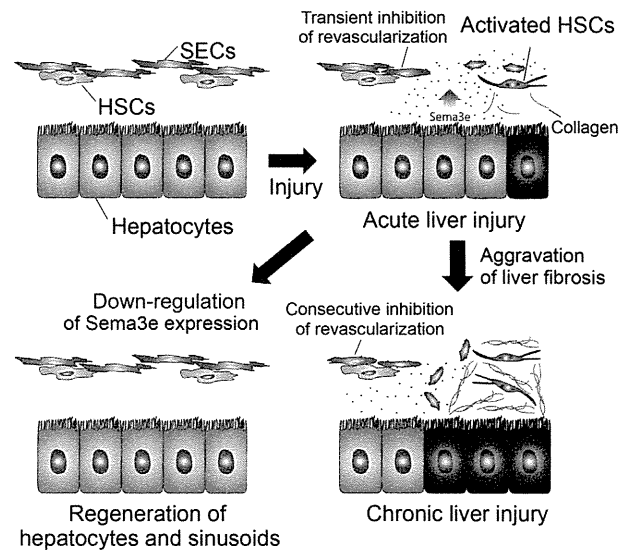


**Figure 6** A model of the regulatory mechanism of sinusoidal regeneration and liver fibrosis by semaphorin 3E (Sema3e) signaling. Damaged hepatocytes express Sema3e transiently to promote contraction of sinusoidal endothelial cells (SECs), which diminishes the influence by hepatic stellate cells (HSCs). Consequently, isolated HSCs are more easily activated to promote liver regeneration during wound healing. However, consecutive Sema3e expression during chronic liver injury causes sustained inhibition of sinusoidal regeneration and HSC activation, resulting in collagen accumulation.

significant role not only in the regulation of sinusoidal regeneration but also in fibrogenesis through HSCs in a paracrine manner. The Sema3e/Plxnd1 axis counteracts VEGF/VEGFR-2 signaling via a feedback mechanism.[19] Because selective activation of VEGFR-1 on SECs stimulates hepatocyte proliferation *in vivo* and reduces liver damage in mice exposed to $CCl_4$,[32] transient expression of Sema3e may contribute to liver regeneration by skewing VEGFR-2 signaling to VEGFR-1. Alternatively, considering that the activation of SECs and/or HSCs contributes to the proliferation of hepatocytes by producing mitogenic cytokines, the regeneration of hepatocytes may be aberrant in *Sema3e*-KO mice. Although no significant difference was found in hepatocyte proliferation between wild-type and *Sema3e*-KO mice after chronic liver injury, further investigation will be required to make a conclusion.

In terms of physiologic significance of transient Sema3e expression by damaged hepatocytes, its possible role in wound repair will be taken into account. The recruitment of immune cells to a damaged site is a step for wound healing.[33] Macrophages operate as voracious phagocytes, clearing the wound of all matrix and cell debris. Therefore, enhanced permeability and decreased density of sinusoids by Sema3e could contribute to wound repair by facilitating the migration of immune cells to damaged region.

Because a massive volume of blood flows into the liver sinusoids, a fine balance between proangiogenic and antiangiogenic signaling is required for liver homeostasis. For example, VEGF, the primary proangiogenic factor in sinusoidal regeneration, is transiently up-regulated after liver injury.[34] However, constitutive expression of VEGF, which is induced by chronic liver injury, results in aberrant angiogenesis and the development of abnormal vascular architecture that is strongly linked to progressive fibrogenesis.[35] Thus, disrupting the balance leads directly to pathologic changes. Therefore, transient expression of Sema3e by damaged hepatocytes may contribute to the fine-tuning of sinusoidal regeneration and the inhibition of aberrant angiogenesis. Taken together, our results suggest that Sema3e contributes to the initial steps of liver regeneration by providing a scaffold for proliferating hepatocytes through activating HSCs. In addition, progressive fibrogenesis could be caused not only by consecutive expression of a proangiogenic factor but also by an antiangiogenic factor. In conclusion, our findings indicate that Sema3e is the main antiangiogenic player of SECs during liver injury and that consecutive Sema3e expression is a risk factor for liver fibrosis. These results suggest that Sema3e or Plxnd1 could be a therapeutic target in liver fibrosis and cirrhosis.

## Acknowledgments

We thank Dr. Yutaka Yoshida and Dr. Atsushi Kumanogoh for providing *Sema3e*-KO mice, Naoko Miyata for assistance with flow cytometry, Yoshiko Kamiya for mouse and technical assistance, and the members of the Miyajima laboratory for helpful discussion and suggestions.

## Supplemental Data

Supplemental material for this article can be found at *http://dx.doi.org/10.1016/j.ajpath.2014.04.018*.

## References

1. Taub R: Liver regeneration: from myth to mechanism. Nat Rev Mol Cell Biol 2004, 5:836–847
2. Selden AC, Hodgson HJ: Growth factors and the liver. Gut 1991, 32: 601–603
3. Michalopoulos GK, DeFrances MC: Liver regeneration. Science 1997, 276:60–66
4. Raghow R: The role of extracellular matrix in postinflammatory wound healing and fibrosis. FASEB J 1994, 8:823–831
5. Zhang DY, Friedman SL: Fibrosis-dependent mechanisms of hepatocarcinogenesis. Hepatology 2012, 56:769–775
6. Friedman SL, Roll FJ, Boyles J, Bissell DM: Hepatic lipocytes: the principal collagen-producing cells of normal rat liver. Proc Natl Acad Sci U S A 1985, 82:8681–8685
7. DeLeve LD, Wang X, Hu L, McCuskey MK, McCuskey RS: Rat liver sinusoidal endothelial cell phenotype is maintained by paracrine and autocrine regulation. Am J Physiol Gastrointest Liver Physiol 2004, 287:G757–G763
8. Deleve LD, Wang X, Guo Y: Sinusoidal endothelial cells prevent rat stellate cell activation and promote reversion to quiescence. Hepatology 2008, 48:920–930
9. Tanaka H, Leung PS, Kenny TP, Gershwin ME, Bowlus CL: Immunological orchestration of liver fibrosis. Clin Rev Allergy Immunol 2012, 43:220–229
10. Nishina T, Komazawa-Sakon S, Yanaka S, Piao X, Zheng DM, Piao JH, Kojima Y, Yamashina S, Sano E, Putoczki T, Doi T, Ueno T, Ezaki J, Ushio H, Ernst M, Tsumoto K, Okumura K, Nakano H: Interleukin-11 links oxidative stress and compensatory proliferation. Sci Signal 2012, 5:ra5
11. Li F, Huang Q, Chen J, Peng Y, Roop DR, Bedford JS, Li CY: Apoptotic cells activate the "phoenix rising" pathway to promote wound healing and tissue regeneration. Sci Signal 2010, 3:ra13
12. Okabe M, Tsukahara Y, Tanaka M, Suzuki K, Saito S, Kamiya Y, Tsujimura T, Nakamura K, Miyajima A: Potential hepatic stem cells reside in EpCAM+ cells of normal and injured mouse liver. Development 2009, 136:1951–1960
13. Inagaki FF, Tanaka M, Inagaki NF, Yagai T, Sato Y, Sekiguchi K, Oyaizu N, Kokudo N, Miyajima A: Nephronectin is upregulated in acute and chronic hepatitis and aggravates liver injury by recruiting CD4 positive cells. Biochem Biophys Res Commun 2013, 430: 751–756
14. Yazdani U, Terman JR: The semaphorins. Genome Biol 2006, 7:211
15. Zhou Y, Gunput RA, Pasterkamp RJ: Semaphorin signaling: progress made and promises ahead. Trends Biochem Sci 2008, 33:161–170
16. Gu C, Giraudo E: The role of semaphorins and their receptors in vascular development and cancer. Exp Cell Res 2013, 319:1306–1316
17. Gu C, Yoshida Y, Livet J, Reimert DV, Mann F, Merte J, Henderson CE, Jessell TM, Kolodkin AL, Ginty DD: Semaphorin 3E and plexin-D1 control vascular pattern independently of neuropilins. Science 2005, 307:265–268
18. Sakurai A, Gavard J, Annas-Linhares Y, Basile JR, Amornphimoltham P, Palmby TR, Yagi H, Zhang F, Randazzo PA, Li X, Weigert R, Gutkind JS: Semaphorin 3E initiates antiangiogenic signaling through plexin D1 by regulating Arf6 and R-Ras. Mol Cell Biol 2010, 30:3086–3098

19. Kim J, Oh WJ, Gaiano N, Yoshida Y, Gu C: Semaphorin 3E-Plexin-D1 signaling regulates VEGF function in developmental angiogenesis via a feedback mechanism. Genes Dev 2011, 25:1399–1411
20. Nonaka H, Tanaka M, Suzuki K, Miyajima A: Development of murine hepatic sinusoidal endothelial cells characterized by the expression of hyaluronan receptors. Dev Dyn 2007, 236:2258–2267
21. Takase HM, Itoh T, Ino S, Wang T, Koji T, Akira S, Takikawa Y, Miyajima A: FGF7 is a functional niche signal required for stimulation of adult liver progenitor cells that support liver regeneration. Genes Dev 2013, 27:169–181
22. Miyaoka Y, Ebato K, Kato H, Arakawa S, Shimizu S, Miyajima A: Hypertrophy and unconventional cell division of hepatocytes underlie liver regeneration. Curr Biol 2012, 22:1166–1175
23. Reddy GK, Enwemeka CS: A simplified method for the analysis of hydroxyproline in biological tissues. Clin Biochem 1996, 29:225–229
24. Nonaka H, Sugano S, Miyajima A: Serial analysis of gene expression in sinusoidal endothelial cells from normal and injured mouse liver. Biochem Biophys Res Commun 2004, 324:15–24
25. Weddle CC, Hornbrook KR, McCay PB: Lipid peroxidation and alteration of membrane lipids in isolated hepatocytes exposed to carbon tetrachloride. J Biol Chem 1976, 251:4973–4978
26. Wanschel A, Seibert T, Hewing B, Ramkhelawon B, Ray TD, van Gils JM, Rayner KJ, Feig JE, O'Brien ER, Fisher EA, Moore KJ: Neuroimmune guidance cue Semaphorin 3E is expressed in atherosclerotic plaques and regulates macrophage retention. Arterioscler Thromb Vasc Biol 2013, 33:886–893
27. Fukushima Y, Okada M, Kataoka H, Hirashima M, Yoshida Y, Mann F, Gomi F, Nishida K, Nishikawa S, Uemura A: Sema3E-PlexinD1 signaling selectively suppresses disoriented angiogenesis in ischemic retinopathy in mice. J Clin Invest 2011, 121:1974–1985
28. Suzuki K, Tanaka M, Watanabe N, Saito S, Nonaka H, Miyajima A: p75 Neurotrophin receptor is a marker for precursors of stellate cells and portal fibroblasts in mouse fetal liver. Gastroenterology 2008, 135:270–281.e273
29. Passino MA, Adams RA, Sikorski SL, Akassoglou K: Regulation of hepatic stellate cell differentiation by the neurotrophin receptor p75NTR. Science 2007, 315:1853–1856
30. Moriya J, Minamino T, Tateno K, Okada S, Uemura A, Shimizu I, Yokoyama M, Nojima A, Okada M, Koga H, Komuro I: Inhibition of semaphorin as a novel strategy for therapeutic angiogenesis. Circ Res 2010, 106:391–398
31. Liu B, Chen Y, St Clair DK: ROS and p53: a versatile partnership. Free Radic Biol Med 2008, 44:1529–1535
32. LeCouter J, Moritz DR, Li B, Phillips GL, Liang XH, Gerber HP, Hillan KJ, Ferrara N: Angiogenesis-independent endothelial protection of liver: role of VEGFR-1. Science 2003, 299:890–893
33. Martin P, Leibovich SJ: Inflammatory cells during wound repair: the good, the bad and the ugly. Trends Cell Biol 2005, 15:599–607
34. Ishikawa K, Mochida S, Mashiba S, Inao M, Matsui A, Ikeda H, Ohno A, Shibuya M, Fujiwara K: Expressions of vascular endothelial growth factor in nonparenchymal as well as parenchymal cells in rat liver after necrosis. Biochem Biophys Res Commun 1999, 254:587–593
35. Valfre di Bonzo L, Novo E, Cannito S, Busletta C, Paternostro C, Povero D, Parola M: Angiogenesis and liver fibrogenesis. Histol Histopathol 2009, 24:1323–1341

 DOI: 10.1002/eji.201444570 Eur. J. Immunol. 2014. 44: 2638–2647

European Journal of Immunology

# Mature resting Ly6C$^{high}$ natural killer cells can be reactivated by IL-15

*Ai Omi, Yutaka Enomoto, Tsuyoshi Kiniwa, Naoko Miyata and Atsushi Miyajima*

Laboratory of Cell Growth and Differentiation, Institute of Molecular and Cellular Biosciences, University of Tokyo, Tokyo, Japan

Mature NK cells are heterogeneous as to their expression levels of cell surface molecules. However, the functional differences and physiological roles of each NK-cell subset are not fully understood. In this study, we report that based on the Ly6C expression levels, mature C57BL/6 murine NK cells can be subdivided into Ly6C$^{low}$ and Ly6C$^{high}$ subsets. Ly6C$^{high}$ NK cells are in an inert state as evidenced by the production of lower levels of IFN-γ and granzyme B, and they exhibit poorer proliferative potential than Ly6C$^{low}$ NK cells. In addition, adoptive transfer experiments revealed that Ly6C$^{high}$ NK cells are derived from Ly6C$^{low}$ NK cells in the steady state. These results strongly suggest that Ly6C$^{high}$ NK cells are resting cells in the steady state. However, in vitro, Ly6C$^{high}$ NK cells become Ly6C$^{low}$ NK cells with strong effector functions upon stimulation with IL-15. Moreover, Ly6C$^{high}$ NK cells also revert to Ly6C$^{low}$ NK cells in vivo upon injection of the IL-15 inducers polyI:C and CpG. Taken together, these results demonstrate the plasticity of mature NK cells and suggest that Ly6C$^{high}$ NK cells are a reservoir of potential NK cells that allow effective and strong response to infections.

**Keywords:** Innate immunity · Interleukin · Memory · NK cell · Viral infection

Additional supporting information may be found in the online version of this article at the publisher's web-site

## Introduction

NK cells are the third most populous lymphocytes and contribute to innate immune responses as effector cells [1, 2]. NK cells are distributed throughout the body, in both lymphoid and nonlymphoid organs, for participation in immune surveillance of tumors or viral infection [1, 3, 4]. Among their various functions, NK cells play major roles in cytotoxicity and the production of inflammatory cytokines such as IFN-γ [1, 3, 4]. Unlike B and T lymphocytes, NK cells do not express a rearranged Ag-specific receptor, but express many types of activating and inhibitory receptors that recognize target cells [2–4]. Cross-linking of these receptors by their ligands regulates the functions of NK cells, and activated NK cells secrete large amounts of IFN-γ and cytotoxic granules containing perforin and granzyme B [1, 3]. Given these features, NK cells have been classified as group 1 innate lymphoid cells [5].

NK cells are differentiated from hematopoietic stem cells and develop in mainly the BM [6]. In mice, NK-cell progenitors express CD122, which is the common subunit of IL-2R and IL-15R [6]. NK cells in the early developmental stage express NK1.1 and NKG2D, followed by the expression of inhibitory and activating receptors such as those in the CD94-NKG2 family or LY49 family [6]. Thereafter, NK cells in the late developmental stage express CD11b at high levels and become mature NK cells [6]. Thus, NK cells show different expression patterns of these surface markers during development and maturation.

Mature NK cells were originally described as a homogenous cell population characterized by their ability to mediate spontaneous

*Correspondence:* Dr. Yutaka Enomoto
e-mail: yenomoto@iam.u-tokyo.ac.jp

 

cytotoxicity against target cells [7–9]. However, in the early 1980s it was proposed that human mature NK cells in peripheral blood can be subdivided into two functional subsets based on the expression of CD56 [10]. $CD56^{dim}$ and $CD56^{bright}$ NK cells exhibit clearly distinct effector functions; that is, $CD56^{dim}$ NK cells posess high cytotoxic capacity, while $CD56^{bright}$ NK cells produce a large amount of cytokines [11–13]. However, as CD56 is not expressed in mice, it has been difficult to identify functionally distinct NK-cell subsets in mice. Recently, efforts have been made to find cell surface markers that can be used to characterize mature murine NK cells and several candidate molecules such as CD27, KLRG1, and CD94 have been found. These studies revealed that mature murine NK cells can be also subdivided into subsets [14–16]. However, their functional differences and physiological roles of each subset remain elusive.

To address this question, we searched for a better marker that can be used to characterize mature NK cells. In the present study, we report that mature murine NK cells ($NK1.1^+CD11b^+CD3e^-$) can be subdivided according to their Ly6C expression levels into $Ly6C^{low}$ and $Ly6C^{high}$ subsets. Ly6C is a member of the Ly6 superfamily and is a glycosylphosphatidylinositol-anchored cell surface molecule [17]. Ly6C is expressed mainly in lymphocytes, monocytes/macrophages, granulocytes, and endothelial cells, and is a useful marker to distinguish the various developmental stages of these cells [18–20]. Moreover, it is well known that memory $CD8^+$ T cells as well as activated $CD8^+$ T cells express higher levels of Ly6C than naive cells [2, 20, 21]. Therefore, Ly6C is often used as a maker of activation and memory in T cells. Both NK cells and $CD8^+$ T cells are derived from a common lymphoid progenitor, and have many common features [2, 22]. However, the characteristics of $Ly6C^{low}$ and $Ly6C^{high}$ NK-cell subsets are not fully understood [23]. We found that there are two states in mature murine NK cells; that is, $Ly6C^{low}$ NK cells are active state and $Ly6C^{high}$ NK cells are resting, respectively. Furthermore, we herein describe the plasticity of mature NK cells.

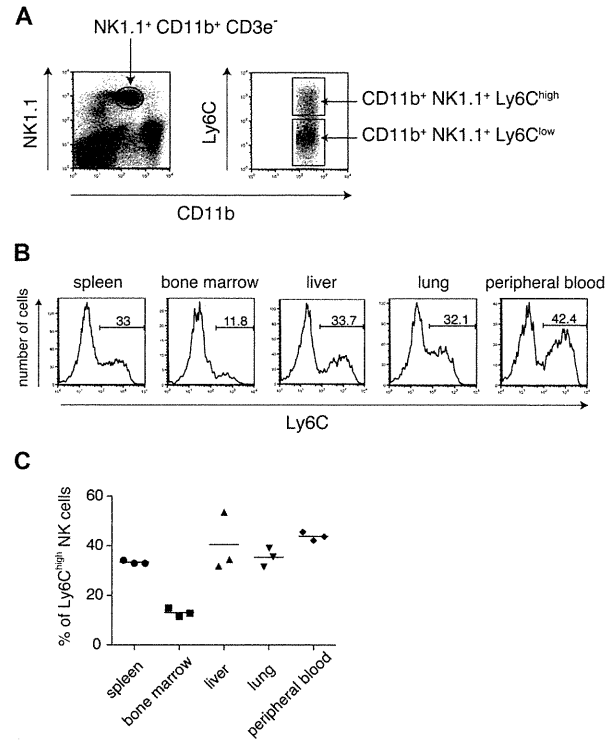


**Figure 1.** Ly6C expression on mature murine NK cells. (A) Cells were isolated from the spleen of C57BL/6 mice and Ly6C expression was assessed by flow cytometry. The dot plots of the right panel were gated on $NK1.1^+CD11b^+CD3e^-$ cells. (B) Cells were isolated from the spleen, BM, liver, lung, and peripheral blood of C57BL/6 mice and Ly6C expression was determined by flow cytometry, gating on $NK1.1^+CD11b^+CD3e^-$ cells. (C) The percentages of $Ly6C^{high}$ NK cells, as determined in (B), in each tissue are shown. Each symbol represents an individual mouse and bars represent the means within the groups ($n = 3$). $p$-value was calculated with one-way ANOVA method followed by Tukey's studentized range test to elucidate the group differences. BM versus spleen, liver, lung, peripheral blood: $p < 0.01$. (A and B) Data shown are from a single experiment representative of three independent experiments performed.

## Results

### Surface expression of Ly6C defines two subsets of mature murine NK cells

We found that mature murine NK cells ($NK1.1^+CD11b^+CD3e^-$) in the spleen can be subdivided into two populations based on the expression levels of Ly6C (Fig. 1A and B). Immature NK cells ($NK1.1^+CD11b^-CD3e^-CD27^+$) [24] were also subdivided by the expression of Ly6C, though the population of Ly6C-expressing cells was very small (Supporting Information Fig. 1).

To reveal the tissue distribution of the $Ly6C^{low}$ and $Ly6C^{high}$ subsets in mature NK cells in vivo, we examined the abundance of each NK-cell subset in lymphoid and nonlymphoid organs, such as the spleen, BM, liver, lung, and peripheral blood by flow cytometry (Fig. 1B). Although both $Ly6C^{low}$ and $Ly6C^{high}$ NK-cell subsets were found in various peripheral tissues, a majority of NK cells in the BM, in which NK cells develop [6], expressed Ly6C at low levels (Fig. 1B and C). These results indicate that the $Ly6C^{high}$ NK-cell subset is present mainly in peripheral tissues.

### Distinct expression patterns of surface markers in NK-cell subsets

NK cells express various activating and inhibitory receptors, and their expression patterns are closely coupled to NK-cell functions [2–4]. Thus, we examined the surface expression of NK-cell receptors on $Ly6C^{low}$ and $Ly6C^{high}$ NK cells by flow cytometry (Fig. 2A and B). The expression levels of activating receptors were similar between $Ly6C^{low}$ and $Ly6C^{high}$ NK-cell subsets with the exception of Ly49H (Fig. 2A). In contrast, $Ly6C^{high}$ NK cells displayed higher proportions of cells expressing the inhibitory receptors KLRG1 and Ly49C/I than did $Ly6C^{low}$ NK cells (Fig. 2B). Conversely, the Ly49A expression levels of $Ly6C^{low}$ NK cells were slightly higher than those of $Ly6C^{high}$ NK cells (Fig. 2B). Furthermore, we investigated

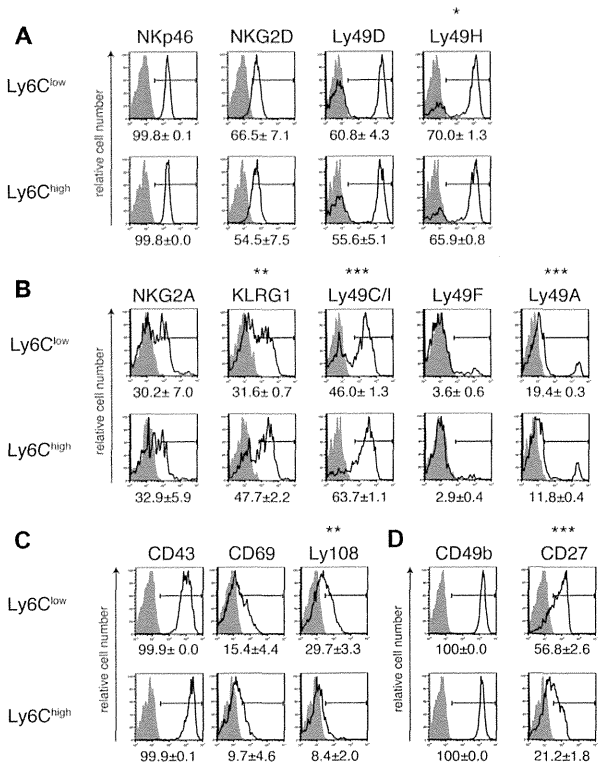


**Figure 2.** Characterization of surface markers on Ly6C$^{low}$ and Ly6C$^{high}$ NK-cell subsets. (A–D) Cells isolated from the spleens of C57BL/6 mice were stained for the indicated cell surface markers. Ly6C$^{low}$ and Ly6C$^{high}$ NK-cell subsets were gated on NK1.1$^+$CD11b$^+$CD3e$^-$ cells. Shaded histograms indicate isotype control. The numbers under each histogram show the mean (±SEM) percentages of positive cells for surface marker expression calculated from three mice and the histograms are representative of three independent experiments performed. $^*p < 0.05$, $^{**}p < 0.01$, $^{***}p < 0.001$ (Student's two-tailed *t*-test).

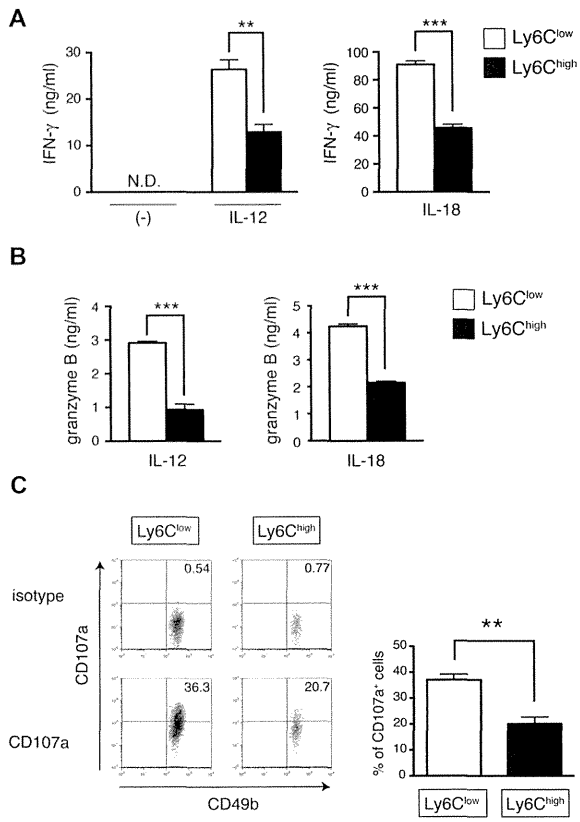


**Figure 3.** IFN-γ production and granzyme B secretion of Ly6C$^{low}$ NK cells and Ly6C$^{high}$ NK cells. (A and B) CD49b$^+$CD11b$^+$CD3e$^-$Ly6C$^{low}$ NK cells and CD49b$^+$CD11b$^+$CD3e$^-$Ly6C$^{high}$ NK cells were sorted from the spleens of C57BL/6 mice. Sorted NK-cell subsets ($5 \times 10^4$ cells/well) were stimulated with IL-12 (100 ng/mL) or IL-18 (100 ng/mL) in the presence of IL-2 (100 ng/mL). After 24 h of incubation, the levels of (A) IFN-γ and (B) granzyme B in the culture supernatants were measured by ELISA. Data are shown as means + SEM of three samples. (C) CD49b$^+$ NK cells were cultured with IL-18 (100 ng/mL) in the presence of IL-2 (100 ng/mL). After 16 h of incubation, NK cells were cocultured with YAC-1 cells by an E:T ratio of 1:1. The dot plot represents the percentage of CD107a$^+$ cells gated on CD49b$^+$CD11b$^+$CD3e$^-$ Ly6C$^{low}$ or Ly6C$^{high}$ NK cells. The bar graphs represent the means (+SEM) percentages of CD107a$^+$ cells ($n = 3$). All data shown are from a single experiment representative of three independent experiments performed. $^{**}p < 0.01$, $^{***}p < 0.001$. N.D., not detected (Student's two-tailed *t*-test).

activation markers known to be upregulated in activated NK cells [25–28] and found that the expression levels of Ly108 were significantly lower in Ly6C$^{high}$ NK cells than in Ly6C$^{low}$ NK cells (Fig. 2C). Taken together, these results suggest that the activity of Ly6C$^{high}$ NK cells is lower than that of Ly6C$^{low}$ NK cells. We next examined the expression of maturation markers in NK cells, namely CD49b and CD27 [6, 14, 24]. CD49b was highly expressed in both Ly6C$^{low}$ and Ly6C$^{high}$ NK cells (Fig. 2D), whereas Ly6C$^{high}$ NK cells displayed lower proportions of cells expressing CD27 than did Ly6C$^{low}$ NK cells (Fig. 2D). This result implies that the maturation stage of Ly6C$^{low}$and that of Ly6C$^{high}$ NK cells are different. While it has been known that CD27 subdivides mature murine NK cells into two populations, our results suggest that the expression of Ly6C did not match the expression of CD27 completely.

## Ly6C$^{high}$ cells are inert NK cells

NK cells have various functions in the immune system. Among them, IFN-γ production and cytotoxicity play major roles for the clearance of infectious pathogens and tumor cells [1, 3, 4]. Therefore, we next examined IFN-γ production by each NK-cell subset. NK cells are known to produce IFN-γ in response to IL-12 or IL-18, which are secreted by APCs such as DCs [1, 29]. As shown in Figure 3A, both NK-cell subsets secreted IFN-γ in response to IL-12 or IL-18. However, IFN-γ secretion by Ly6C$^{high}$ NK cells was approximately half that of Ly6C$^{low}$ NK cells (Fig. 3A). In order to exclude the possibility that viability of NK-cell subsets were different during the assay, IL-2 was added to maintain the survival of NK cells [30, 31]. Subsequently, there was no difference in cell viability between Ly6C$^{low}$ and ly6C$^{high}$ NK cells (data not shown). Activated NK cells release cytotoxic granules containing perforin and granzyme B to kill target cells [1, 3]. Granzyme

B directly cleaves caspases and activates the apoptotic-signaling pathway in target cells [32, 33]. To evaluate the cytotoxic capability of each NK-cell subset, we examined the secretion of granzyme B in response to IL-12 or IL-18. Production of granzyme B by Ly6C$^{high}$ NK cells was lower than that by Ly6C$^{low}$ NK cells when stimulated with IL-12 or IL-18 (Fig. 3B). In addition, we examined CD107a expression in each NK-cell subset when cocultured with YAC-1 cells. CD107a is a glycoprotein present in the membrane of cytotoxic granules and exposed on the surface of activated NK cells [34]. Consistent with granzyme B productions, the percentage of CD107a$^+$ cells in Ly6C$^{high}$ NK cells was lower than that in Ly6C$^{low}$ NK cells when stimulated with IL-18 (Fig. 3C). These data collectively indicate that Ly6C$^{low}$ NK cells exhibit stronger NK functions than do Ly6C$^{high}$ NK cells in response to cytokine stimulation. These results correlated with our finding that Ly6C$^{high}$ NK cells express higher levels of KLRG1, Ly49C/I, and lower levels of Ly108 (Fig. 2B). Therefore, Ly6C$^{high}$ NK cells are thought to be refractory to cytokine stimulation.

## Ly6C$^{low}$ NK cells become Ly6C$^{high}$ NK cells in the steady state

We next investigated the interrelationship of Ly6C$^{low}$ and Ly6C$^{high}$ NK cells. To determine whether these NK-cell subsets are interconvertible, we performed an in vivo transplantation assay. NK-cell subsets were sorted from the spleens of CD45.2 C57BL/6J (C57BL/6) mice and adoptively transferred into nonirradiated CD45.1 congenic mice by i.v. injection. Two weeks after the transplantation, we isolated the transferred CD45.2$^+$ NK cells from the spleen and examined their expression levels of Ly6C. Approximately 30% of CD45.2$^+$ NK cells in mice that received Ly6C$^{low}$ NK cells were Ly6C$^{high}$, indicating that a significant portion of the transferred Ly6C$^{low}$ NK cells were converted to Ly6C$^{high}$ NK cells (Fig. 4A and B). In contrast, almost all transferred Ly6C$^{high}$ NK cells did not change their high expression levels of Ly6C (Fig. 4A and B). These results suggest that Ly6C$^{low}$ NK cells become Ly6C$^{high}$ NK cells, but not vice versa in the steady state.

## IL-15 converts Ly6C$^{high}$ NK cells to Ly6C$^{low}$ NK cells

IL-15 is a major cytokine required for the development and proliferation of NK cells [31, 35, 36]. To determine whether IL-15 affects the Ly6C expression levels of NK cells, both Ly6C$^{low}$ and Ly6C$^{high}$ NK cells were sorted and cultured with IL-15. First, we determined the absolute cell number of Ly6C$^{low}$ and Ly6C$^{high}$ NK cells. After 6-day culture, both subsets survived and Ly6C$^{low}$ NK cells showed significantly higher proliferative potential than Ly6C$^{high}$ NK cells (Fig. 5A). Next, we examined the expression levels of Ly6C at indicated time points. The Ly6C expression levels in Ly6C$^{low}$ NK cells remained unchanged (Fig. 5B, left panel). Interestingly, however, the Ly6C expression levels of Ly6C$^{high}$ NK cells gradually decreased, and about a half of the NK cells expressed Ly6C at

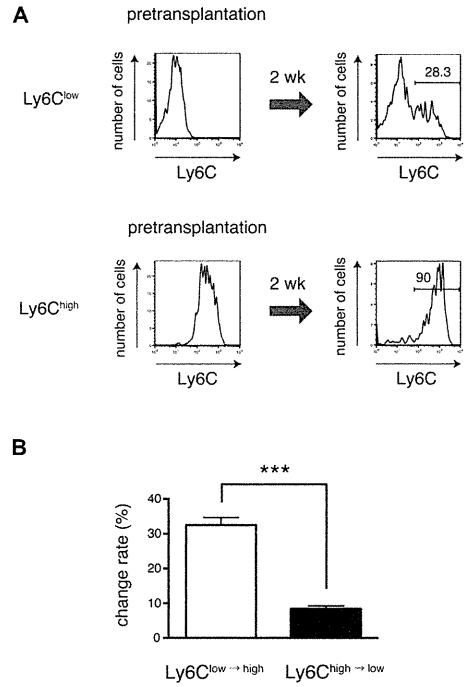


**Figure 4.** Ly6C$^{high}$ NK cells are derived from Ly6C$^{low}$ NK cells. (A and B) CD49b$^+$CD11b$^+$CD3e$^-$Ly6C$^{low}$ NK cells and CD49b$^+$CD11b$^+$CD3e$^-$Ly6C$^{high}$ NK cells were sorted from the spleen of CD45.2 C57BL/6 mice and transferred into nonirradiated CD45.1 congenic mice. Two weeks later, cells were harvested from the spleens of the recipient mice, stained for CD49b, CD11b, CD3e, CD45.2, and Ly6C and analyzed by flow cytometry. (A) The histogram plots show Ly6C expression profiles gated on CD49b$^+$CD11b$^+$CD3e$^-$CD45.2$^+$ cells. Numbers indicate percentage of Ly6C-positive cells. Data shown are from a single experiment representative of three independent experiments performed. (B) The graph indicates change rate of each subset (i.e., the percentage of Ly6C$^{high}$ NK cells derived from Ly6C$^{low}$ NK cells or Ly6C$^{low}$ NK cells derived from Ly6C$^{high}$ NK cells). Data shown are the means + SEM of three independent experiments performed. These data were compared using Student's two-tailed t-test. ***$p < 0.001$.

middle levels (Ly6C$^{mid(high)}$ NK cells) when cultured with IL-15 for 4 days, and finally many NK cells became Ly6C$^{low}$ NK cells after 6 days in culture with IL-15 (Fig. 5B, right panel). Furthermore, we examined the effect of IL-2 on the expression levels of Ly6C, as IL-2 and IL-15 share the common cytokine-receptor gamma chain and IL-2 is also a major cytokine required for the development and proliferation of NK cells. After 6-day culture with IL-2, both subsets survived and Ly6C$^{low}$ NK cells showed significantly higher proliferative capacity than Ly6C$^{high}$ NK cells (Supporting Information Fig. 2A). Ly6C expression levels of Ly6C$^{high}$ NK cells decreased and approximately half of the NK cells expressed Ly6C at intermediate levels (Supporting Information Fig. 2B). These results suggest that IL-2 also has the effect to convert Ly6C$^{high}$ NK cells to Ly6C$^{low}$ NK cells. However, the effect of IL-2 was not so strong as that of IL-15. Because the functions of the Ly6C$^{low}$ NK cells were higher than those of the Ly6C$^{high}$ NK cells (Fig. 3), we analyzed the effector functions of Ly6C$^{low}$ NK cells derived from Ly6C$^{low}$ NK cells (Ly6C$^{low(low)}$ NK cells) and of Ly6C$^{mid(high)}$ NK cells or Ly6C$^{low}$

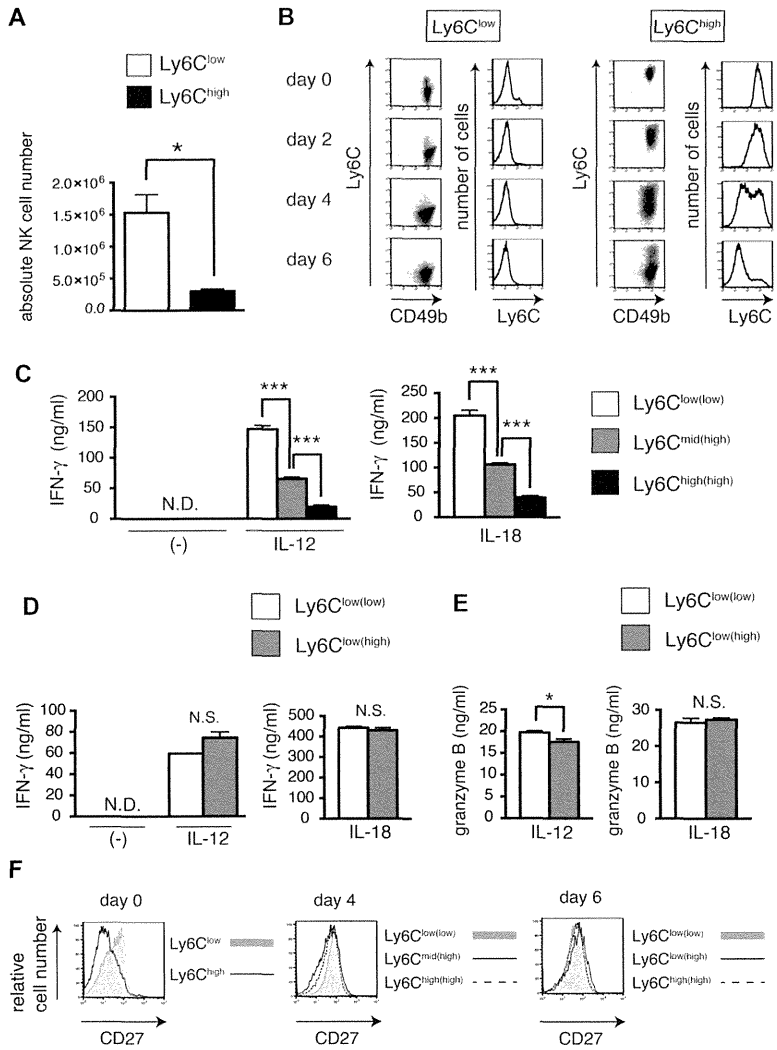


**Figure 5.** Conversion of Ly6C$^{high}$ NK cells to Ly6C$^{low}$ NK cells. (A) CD49b$^+$CD11b$^+$CD3e$^-$Ly6C$^{low}$ NK cells and CD49b$^+$CD11b$^+$CD3e$^-$Ly6C$^{high}$ NK cells ($3 \times 10^5$) were cultured with IL-15 (100 ng/mL) for 6 days and absolute cell number was determined in triplicate cultures by using a 0.4% Trypan blue solution. Data are shown as means + SEM of three samples from a single experiment representative of three independent experiments. (B) CD49b$^+$CD11b$^+$CD3e$^-$Ly6C$^{low}$ NK cells and CD49b$^+$CD11b$^+$CD3e$^-$Ly6C$^{high}$ NK cells were cultured with IL-15 (100 ng/mL) for the indicated time periods. During each time period, cells were harvested and stained for CD49b, CD11b, CD3e, and Ly6C. Data shown are from a single experiment representative of three independent experiments performed. (C) NK-cell subsets were cultured with IL-15 (100 ng/mL) for 4 days. Ly6C$^{low(low)}$ NK cells, Ly6C$^{mid(high)}$ NK cells, and Ly6C$^{high(high)}$ NK cells were sorted by cell sorter and stimulated with IL-12 (100 ng/mL) or IL-18 (100 ng/mL) in the presence of IL-2 (100 ng/mL) ($2 \times 10^4$ cells/well). After 24 h of incubation, the levels of IFN-γ in the culture supernatants were measured by ELISA. Data are shown as means + SEM of three samples from a single experiment representative of three independent experiments. (D, E) NK-cell subsets were cultured with IL-15 (100 ng/mL) for 7 days. Ly6C$^{low(low)}$ NK cells and Ly6C$^{low(high)}$ NK cells were then sorted and stimulated with IL-12 (100 ng/mL) or IL-18 (100 ng/mL) in the presence of IL-2 (100 ng/mL) ($2 \times 10^4$ cells/well). After 24 h of incubation, the levels of (D) IFN-γ and (E) granzyme B in the culture supernatants were measured by ELISA. Data are shown as means + SEM of three samples from a single experiment representative of three independent experiments. (F) NK-cell subsets were cultured with IL-15 (100 ng/mL) for 4 or 6 days. The histogram plots show CD27 expression profiles gated on CD49b$^+$CD3e$^-$Ly6C$^{low/mid/high}$ cells. Data shown are a representative of two independent experiments. $^*p < 0.005$, $^{***}p < 0.001$. N.D., not detected, N.S., not significant (Student's two-tailed t-test).

NK cells derived from Ly6C$^{high}$ NK cells (Ly6C$^{low(high)}$ NK cells) 4 days or 1 week in culture with IL-15, respectively. We found that the ability of Ly6C$^{mid(high)}$ NK cells to secrete IFN-γ was lower than that of Ly6C$^{low(low)}$ NK cells in response to IL-12 or IL-18 (Fig. 5C). Notably, approximately half of the Ly6C$^{high}$ NK cells retained high expression levels of Ly6C (Ly6C$^{high(high)}$ NK cells) 4 days in culture with IL-15, and the production of IFN-γ of Ly6C$^{mid(high)}$ NK cells was higher than Ly6C$^{high(high)}$ NK cells (Fig. 5C). The ability of Ly6C$^{low(high)}$ NK cells to secrete IFN-γ and granzyme B was increased to levels comparable to that of Ly6C$^{low(low)}$ NK cells for 1 week in the presence of IL-15 (Fig. 5D and E). As stated above, Ly6C$^{high}$ NK cells displayed lower proportions of cells expressing CD27 than did Ly6C$^{low}$ NK cells before culture with IL-15 (Fig. 2D). We therefore examined CD27 expression levels of both Ly6C$^{low}$ and Ly6C$^{high}$ NK cells in culture with IL-15 for 4 days, and found no differences in the expression levels of CD27 among the three populations of Ly6C$^{low(low)}$, Ly6C$^{mid(high)}$, and Ly6C$^{high(high)}$ NK cells (Fig. 5F). Furthermore, after 6 days in culture, there was also no difference in the expression levels of CD27 among the three populations, Ly6C$^{low(low)}$, Ly6C$^{low(high)}$, and Ly6C$^{high(high)}$ NK cells. These results indicate that the expression levels of CD27 are not well correlated with activity of mature NK cells.

## Conversion of Ly6C$^{high}$ NK cells to Ly6C$^{low}$ NK cells in vivo

We next examined whether Ly6C$^{high}$ NK cells could become Ly6C$^{low}$ NK cells in vivo. Because IL-15 was shown to convert Ly6C$^{high}$ NK cells into Ly6C$^{low}$ NK cells in vitro (Fig. 5B), we first performed an in vivo transplantation assay by overexpressing IL-15 in mice. To express IL-15 in vivo, we utilized the hydrodynamic tail vein injection method [37–39]. NK-cell subsets were sorted from the spleens of CD45.2 C57BL/6 mice and adoptively transferred into CD45.1 congenic mice injected with control vector

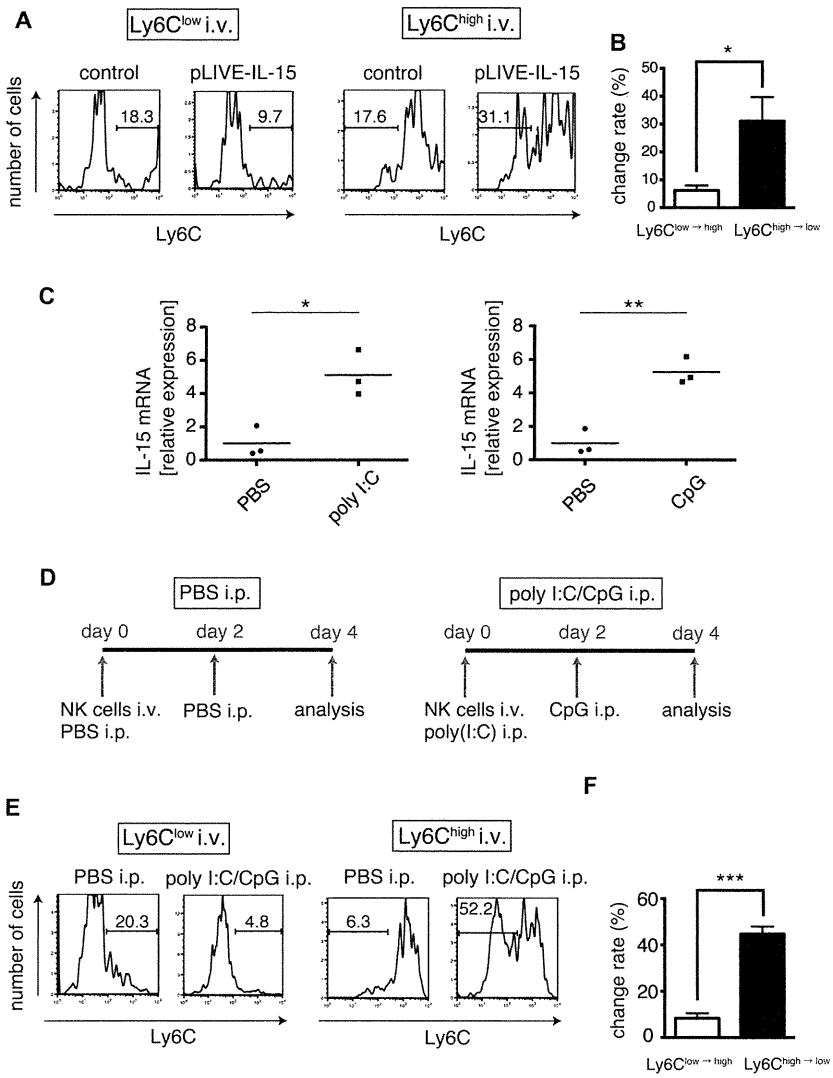


**Figure 6.** Conversion of Ly6C$^{high}$ NK cells to Ly6C$^{low}$ NK cells in vivo. (A and B) control vector or pLIVE-IL-15 (20 μg) were injected i.v. into CD45.1 congenic mice. Six hours after injection, NK-cell subsets ($3 \times 10^5$ to $5 \times 10^5$cells) from the spleens of CD45.2 C57BL/6 mice were transferred into these CD45.1 mice. Four days later, cells were harvested from the spleens of the recipient mice, stained for CD49b, CD11b, CD3e, CD45.2, and Ly6C and analyzed by flow cytometry. The histogram plots show Ly6C expression profiles gated on CD49b$^+$CD11b$^+$CD3e$^-$CD45.2$^+$ cells. Numbers indicate percentages. Plots are representative of three independent experiments. (B) Change rate of each subset described in (A) ($n$ = 4). (C) C57BL/6 mice were injected i.p. with PBS, 100 μg of polyI:C, or 20 nmol of CpG. After 3 h, splenocytes from these C57BL/6 mice were harvested. Expression of IL-15 mRNA was determined by real-time RT-PCR. The expression levels were normalized to HPRT. Each symbol represents an individual mouse and bars represent the means within the groups. Data are pooled from three independent experiments. (D) NK-cell subsets were sorted from the spleens of CD45.2 C57BL/6 mice and transferred into nonirradiated CD45.1 congenic mice. These mice were then injected i.p. with polyI:C (day 0) and CpG (day 2) or PBS (day 0 and day 2) ($n$ = 3). Splenocytes were harvested from the recipient mice transferred with Ly6C$^{low}$ NK cells and Ly6C$^{high}$ NK cells. Cells were stained for CD49b, CD11b, CD3e, CD45.2, and Ly6C and assessed by flow cytometry. (E) Histograms show Ly6C expression profiles gated on CD49b$^+$CD11b$^+$CD3e$^-$CD45.2$^+$ cells. Numbers indicate percentages. (F) The graph indicates change rate of each subset in the mouse treated with both poly I:C and CpG as described in (E). Data are shown as means + SEM of three independent experiments performed. $^*p < 0.05$, $^{**}p < 0.01$, $^{***}p < 0.001$ (Student's two-tailed t-test). i.p., intraperitoneal injection, i.v., intravenous injection.

or pLIVE-IL-15 vector. Four days posttransplantation, we isolated the transferred CD45.2 NK cells from the spleen and examined their expression levels of Ly6C. Flow cytometric analysis showed that approximately 30% of the transferred Ly6C$^{high}$ NK cells in the mouse injected with pLIVE-IL-15 were converted to Ly6C$^{low}$ NK cells (Fig. 6A and B). In contrast, the transferred Ly6C$^{high}$ NK cells in the mouse injected with control vector and the transferred Ly6C$^{low}$ NK cells remained unchanged (Fig. 6A and B). We next examined the conversion during immune responses. Because DCs are known to trans-present IL-15 to NK cells when activated by viral infection or TLR ligands such as polyI:C and CpG [40–42], we evaluated the expression of IL-15 in splenocytes harvested from mice i.p. injected with polyI:C or CpG. Real-time RT-PCR analysis demonstrated that IL-15 was significantly increased in splenocytes when stimulated with polyI:C or CpG (Fig. 6C). Next, we transferred NK-cell subsets sorted from the spleens of CD45.2 C57BL/6 mice into nonirradiated CD45.1 congenic mice that had been injected i.p. with polyI:C or both polyI:C and CpG (Fig. 6D and Supporting Information Fig. 3A). Administration of both polyI:C and CpG mimics severe viral infection, and these two different TLR ligands are assumed to activate DCs synergistically [43, 44]. We then analyzed transferred NK cells in the spleen of the recipient mouse after i.p. injection of polyI:C or both polyI:C and CpG. Flow cytometric analysis indicated that approximately 30% or half of the transferred Ly6C$^{high}$ NK cells in the mouse treated with polyI:C or both polyI:C and CpG, respectively, were converted to Ly6C$^{low}$ NK cells (Supporting Information Fig. 3B and C and Fig. 6E and F). In contrast, the transferred Ly6C$^{high}$ NK cells in the mouse treated with PBS and the transferred Ly6C$^{low}$ NK cells remained unchanged (Fig. 6E and F). Collectively, these results indicate that mature NK cells can change their phenotype in response to the environment.

## Discussion

In the human, mature NK cells are subdivided into two populations based on the expression levels of CD56. These two subsets, $CD56^{dim}$ and $CD56^{bright}$ NK cells, play clearly distinct roles in terms of their effector functions; that is, $CD56^{dim}$ NK cells produce low levels of IFN-γ but exhibit a high cytotoxic capacity, while $CD56^{bright}$ NK cells produce a large amount of IFN-γ but exhibit a weak cytotoxic capacity [11–13, 45]. In mice, it has been shown that mature NK cells are divided in two populations based on the CD27 expression levels and that $CD27^{low}$ NK cells are derived from $CD27^{high}$ NK cells, and exhibit lower activity than $CD27^{high}$ NK cells [14, 24]. However, the two subsets of mature NK cells in human and mouse are not the same and physiological roles of those NK subsets remain unknown. In this study, we found that mature murine NK cells are subdivided into two subsets, $Ly6C^{low}$ and $Ly6C^{high}$ NK cells, based on the expression levels of Ly6C and characterized their functions and relationship.

NK cells play major roles for host protection against infectious pathogens and tumor cells at an early stage by IFN-γ production and cytotoxicity [1, 3, 4]. We demonstrated that $Ly6C^{high}$ NK cells produced lower levels of both IFN-γ and cytotoxic granules than did $Ly6C^{low}$ NK cells, correlating with the surface phenotype of $Ly6C^{high}$ NK cells that express higher levels of inhibitory receptors. Moreover, the proliferative potential of $Ly6C^{high}$ NK cells was lower than that of $Ly6C^{low}$ NK cells when cultured with IL-15. Lower effector functions and proliferation potential suggest that $Ly6C^{high}$ NK cells are in an inert state compared with $Ly6C^{low}$ NK cells. While the frequency of $Ly6C^{high}$ NK cells in the spleen, liver, lung, and peripheral blood was almost the same, it was significantly low in the BM where NK cells derive. Moreover, adoptive transfer of each subset showed that $Ly6C^{high}$ NK cells are derived from $Ly6C^{low}$ NK cells. These results imply that $Ly6C^{high}$ NK cells in peripheral tissues are resting cells. These results are similar to the previous study showing that $CD27^{low}$ NK cells are derived from $CD27^{high}$ NK cells, and exhibit lower activity than $CD27^{high}$ NK cells [14]. However, a major finding in our study is that inert $Ly6C^{high}$ NK cells can be reactivated.

We found that $Ly6C^{high}$ NK cells can be converted to $Ly6C^{low}$ NK cells ($Ly6C^{low(high)}$ NK cells) when cultured with IL-15. The expression levels of Ly6C also decreased when cultured with IL-2, but the effect of IL-2 was not as strong as IL-15. Moreover, the ability of $Ly6C^{low(high)}$ NK cells to secrete IFN-γ and granzyme B was increased to the level comparable to that of $Ly6C^{low}$ NK cells cultured with IL-15 ($Ly6C^{low(low)}$ NK cells). This conversion of $Ly6C^{high}$ NK cells to $Ly6C^{low}$ NK cells was also shown in vivo by overexpression of IL-15 or by the administration of polyI:C and CpG, potent inducers of IL-15. These results suggest that under the steady-state conditions, $Ly6C^{low}$ NK cells with strong activity develop in the BM and become resting $Ly6C^{high}$ NK cells. However, those resting NK cells are reactivated when IL-15 expression level is increased, for example, by virus infection. Thus, the present study suggests that $Ly6C^{high}$ NK cells are a reservoir of potential NK cells that allow effective and strong response to infections.

Ly6C is known to be expressed in lymphocytes, monocytes/macrophages, granulocytes, and endothelial cells [18–20]. Although its function is not completely understood, Ly6C shows distinct expression patterns in the different developmental stages of these cells. Interestingly, naive $CD8^+$ T cells express Ly6C at low levels, but $CD8^+$ memory T cells express Ly6C at high levels [2, 20, 21]. There are many common features between NK cells and $CD8^+$ T cells [2, 22]. Both NK cells and $CD8^+$ T cells are derived from a common lymphoid progenitor, and their development and/or maintenance is regulated by IL-15. In addition, they release perforin and granzyme B in cytotoxic granules and produce a large amount of IFN-γ during viral infection or in response to proinflammatory cytokines such as IL-12. In general, $CD8^+$ memory T cells become long-lived resting cells after the first immune response and can be reactivated by encountering the same Ag [46, 47]. Considering that the functions of $Ly6C^{high}$ NK cells are suppressed in the steady state but can be reactivated by immunological stimuli, $Ly6C^{high}$ NK cells might be similar to $CD8^+$ memory T cells expressing Ly6C.

NK cells have traditionally been classified as effector cells in the innate immune system. However, a recent report showed that NK cells also possess memory function and contribute to the adaptive immune system [48, 49]. After mouse cytomegalovirus (MCMV) infection, NK cells bearing the virus-specific Ly49H receptor resided in lymphoid and nonlymphoid organs for several months [49]. These memory NK cells were reactivated, rapidly degranulated, and produced cytokines by secondary viral challenge. Interestingly, these memory NK cells showed higher expression of Ly6C. Moreover, the same group indicated that adoptive transfer of mature NK cells into lymphopenic mice resulted in the generation of long-lived NK cells [50]. These NK cells resided in both lymphoid and nonlymphoid organs for more than 6 months, retained their functionality many months after initial transfer, and responded robustly to viral infection. However, the expression levels of Ly6C of long-lived NK cells were not shown. Further studies are necessary to uncover the mechanism of differentiation of $Ly6C^{low}$ NK cells into $Ly6C^{high}$ NK cells and address whether $Ly6C^{high}$ NK cells are long-lived NK cells, memory NK cells, or their progenitors. While our results showed that different stages of NK cells are distinguishable by the Ly6C expression levels, the role of Ly6C in NK-cell function remains unknown.

In conclusion, we showed that resting $Ly6C^{high}$ NK cells are present in WT mice in the steady state, and that these $Ly6C^{high}$ NK cells can be reactivated by IL-15.

## Materials and methods

### Mice

WT C57BL/6J (C57BL/6) mice were purchased from CLEA Japan, Inc. CD45.1 congenic C57BL/6 mice (RBRC 00144) were provided by RIKEN BRC through the National Bio-Resource Project of the MEXT, Japan. All mice were maintained under standard

specific pathogen free (SPF) conditions and used between 10 and 14 weeks of age. The animal studies were performed according to the guidelines set by the Institutional Animal Care and Use Committee of the University of Tokyo.

### Flow cytometric analysis

RBC-depleted cells were stained for the following antibodies: brilliant violet 421-conjugated anti-CD3e; FITC-conjugated anti-CD11b; PE-conjugated anti-KLRG1, Ly49H, Ly49D, Ly49A, NKG2A, NK1.1, CD45.1, and CD45.2; PE/Cy7-conjugated anti-Ly6C; biotin-conjugated anti-CD49b, CD27, NKp46, Ly108, and NKG2D; APC-conjugated streptavidin (BioLegend); PE-conjugated anti-CD3e, Ly49C/I, and Ly49F; and biotin-conjugated anti-NK1.1 (BD Pharmingen). The stained cells were analyzed using a FACS Canto II (BD Biosciences) and the FlowJo 8.8.7 software (TreeStar, Ashland, OR).

### Cell culture and proliferation assay in vitro

NK cells ($CD49b^+CD11b^+CD3e^-$) were isolated from the spleens of C57BL/6 mice and further fractionated into $Ly6C^{low}$ and $Ly6C^{high}$ NK cells using a MoFlo cell sorter (Beckman Coulter). Purified $Ly6C^{low}$ and $Ly6C^{high}$ NK cells were cultured in RPMI-1640 medium containing 10% FBS, 2-ME (50 μM), HEPES (20 mM), nonessential AA, sodium pyruvate, L-Gln, and gentamycin in the presence of recombinant mouse IL-15 (100 ng/mL, eBioscience) or IL-2 (100 ng/mL, PROSPEC). Cell survival was measured in triplicate using the Trypan blue exclusion test.

### ELISA

Purified murine splenic NK cells were stimulated with IL-12 (100 ng/mL, PeproTech) or IL-18 (100 ng/mL, MBL) in the presence of IL-2 (100 ng/mL, PROSPEC). After 24 h of incubation, cell-free supernatants were analyzed using an ELISA kit for IFN-γ (BD Biosciences) or granzyme B (R&D). ELISAs were performed in triplicate.

### CD107a expression

NK cells ($CD49b^+$) were isolated from the spleens of C57BL/6 mice by using MACS (Miltenyi Biotec). Purified NK cells were cultured in the presence of recombinant mouse IL-2 (100 ng/mL) and IL-18 (100 ng/mL). After 16 h incubation, NK cells were stained for CD3e, CD11b, Ly6C, and CD49b. For stimulation steps, NK cells were stained for CD107a and incubated with YAC-1 cells (RCB1165 provided by RIKEN BRC through the National Bio-Resource Project of the MEXT, Japan) by an E:T ratio of 1:1 in the presence of IL-2 (100 ng/mL) and IL-18 (100 ng/mL) for 5 h at 37°C. And then, monensin solution (10 μM, BioLegend) was added during the last 4 h of the culture. Following 5 h incubation, cells were analyzed by FACS Canto II.

### Adoptive cell transfer

Sorted NK cells ($5 \times 10^5$ to $1 \times 10^6$ cells) from the spleens of C57BL/6 mice were injected i.v. into nonirradiated CD45.1 congenic mice. In some experiments, the mice that received NK cells were injected i.p. with polyI:C (100 μg, InvivoGen) and CpG ODN (20 nmol, Hycult Biotech) or PBS.

### Overexpression by hydrodynamic tail vein injection method

Mouse IL-15 cDNA was amplified by PCR: 5′-gcgctagccacca tgaaaattttgaaaccatatatgag-3′ and 5′-cgctcgagtcaggacgtgttgatg aaca-3′, and was inserted into the NheI and XhoI sites of a pLIVE vector (Mirus, Madison, WI). pLIVE-IL-15 (20 μg) was diluted with TransIT-EE Hydrodynamic Delivery Solution (Mirus, Madison, WI) and injected i.v. into CD45.1 congenic mice. pLIVE-SEAP (secreted alkaline phosphatase) (20 μg) was used as a control [39].

### Real-time RT-PCR

C57BL/6 mice were i.p. injected with PBS, polyI:C (100 μg), or CpG ODN (20 nmol). After 3 h, splenocytes from these C57BL/6 mice were harvested and total RNA was prepared using an RNeasy Mini Kit (Qiagen). The total RNA was reverse-transcribed with PrimeScript RT Master Mix (Takara Bio Ink). Quantitative real-time RT-PCR was performed on a LightCycler 480 (Roche Applied Science) using SYBR premix Ex Taq reagent (Takara Bio Ink). HPRT was used as an internal control. The sequence of primers was as follows: 5′-tctcgtgctacttgtgtttccttc-3′ and 5′-catctatccagttggcctctgtt-3′ for IL-15 and 5′-tgacactggtaaaacaat gc-3′ and 5′-tatccaacacttcgagaggt-3′ for HPRT.

### Statistical analysis

Unless otherwise stated, data are shown as means ± SEM and were compared using Student's two-tailed *t*-test. A value of $p < 0.05$ was taken to indicate statistical significance. Statistical analyses were performed using GraphPad Prism (GraphPad Software, San Diego, CA).

Acknowledgments: We would like to thank Dr. Tohru Itoh for providing us with the pLIVE-SEAP vector and pLIVE-IL-15 vector.

 

We would also like to thanks Dr. Cindy Kok for critical reading of the manuscript. This work was supported by research grants from the Ministry of Education, Culture, Sports, Science, and Technology (MEXT) of Japan (No. 22118006), the Ministry of Health, Labour, and Welfare (MHLW) of Japan (H24-hepatitis-general-005), and the Tokyo Biochemical Research Foundation.

Conflict of interest: The authors declare no financial or commercial conflict of interest.

## References

1 Vivier, E., Tomasello, E., Baratin, M., Walzer, T. and Ugolini, S., Functions of natural killer cells. *Nat. Immunol.* 2008. 9: 503–510.

2 Sun, J. C. and Lanier, L. L., NK cell development, homeostasis and function: parallels with CD8(+) T cells. *Nat. Rev. Immunol.* 2011. 11: 645–657.

3 Cerwenka, A. and Lanier, L. L., Natural killer cells, viruses and cancer. *Nat. Rev. Immunol.* 2001. 1: 41–49.

4 Yokoyama, W. M. and Plougastel, B. F., Immune functions encoded by the natural killer gene complex. *Nat. Rev. Immunol.* 2003. 3: 304–316.

5 Spits, H., Artis, D., Colonna, M., Diefenbach, A., Di Santo, J. P., Eberl, G., Koyasu, S. et al., Innate lymphoid cells—a proposal for uniform nomenclature. *Nat. Rev. Immunol.* 2013. 13: 145–149.

6 Kim, S., Iizuka, K., Kang, H. S., Dokun, A., French, A. R., Greco, S. and Yokoyama, W. M., In vivo developmental stages in murine natural killer cell maturation. *Nat. Immunol.* 2002. 3: 523–528.

7 Strowig, T., Brilot, F. and Munz, C., Noncytotoxic functions of NK cells: direct pathogen restriction and assistance to adaptive immunity. *J. Immunol.* 2008. 180: 7785–7791.

8 Herberman, R. B., Nunn, M. E. and Lavrin, D. H., Natural cytotoxic reactivity of mouse lymphoid cells against syngeneic acid allogeneic tumors. I. Distribution of reactivity and specificity. *Int. J. Cancer.* 1975. 16: 216–229.

9 Kiessling, R., Klein, E. and Wigzell, H., "Natural" killer cells in the mouse. I. Cytotoxic cells with specificity for mouse Moloney leukemia cells. Specificity and distribution according to genotype. *Eur. J. Immunol.* 1975. 5: 112–117.

10 Lanier, L. L., Le, A. M., Phillips, J. H., Warner, N. L. and Babcock, G. F., Subpopulations of human natural killer cells defined by expression of the Leu-7 (HNK-1) and Leu-11 (NK-15) antigens. *J. Immunol.* 1983. 131: 1789–1796.

11 Frey, M., Packianathan, N. B., Fehniger, T. A., Ross, M. E., Wang, W. C., Stewart, C. C., Caligiuri, M. A. et al., Differential expression and function of L-selectin on CD56bright and CD56dim natural killer cell subsets. *J. Immunol.* 1998. 161: 400–408.

12 Jacobs, R., Hintzen, G., Kemper, A., Beul, K., Kempf, S., Behrens, G., Sykora, K. W. et al., $CD56^{bright}$ cells differ in their KIR repertoire and cytotoxic features from $CD56^{dim}$ NK cells. *Eur. J. Immunol.* 2001. 31: 3121–3127.

13 Cooper, M. A., Fehniger, T. A., Turner, S. C., Chen, K. S., Ghaheri, B. A., Ghayur, T., Carson, W. E., et al., Human natural killer cells: a unique innate immunoregulatory role for the CD56(bright) subset. *Blood* 2001. 97: 3146–3151.

14 Hayakawa, Y. and Smyth, M. J., CD27 dissects mature NK cells into two subsets with distinct responsiveness and migratory capacity. *J. Immunol.* 2006. 176: 1517–1524.

15 Huntington, N. D., Tabarias, H., Fairfax, K., Brady, J., Hayakawa, Y., Degli-Esposti, M. A., Smyth, M. J. et al., NK cell maturation and peripheral homeostasis is associated with KLRG1 up-regulation. *J. Immunol.* 2007. 178: 4764–4770.

16 Yu, J., Wei, M., Mao, H., Zhang, J., Hughes, T., Mitsui, T., Park, I. K. et al., CD94 defines phenotypically and functionally distinct mouse NK cell subsets. *J. Immunol.* 2009. 183: 4968–4974.

17 Bamezai, A., Mouse Ly-6 proteins and their extended family: markers of cell differentiation and regulators of cell signaling. *Arch. Immunol. Ther. Exp. (Warsz)* 2004. 52: 255–266.

18 Jutila, M. A., Kroese, F. G., Jutila, K. L., Stall, A. M., Fiering, S., Herzenberg, L. A., Berg, E. L., et al., Ly-6C is a monocyte/macrophage and endothelial cell differentiation antigen regulated by interferon-gamma. *Eur. J. Immunol.* 1988. 18: 1819–1826.

19 Jutila, D. B., Kurk, S. and Jutila, M. A., Differences in the expression of Ly-6C on neutrophils and monocytes following PI-PLC hydrolysis and cellular activation. *Immunol. Lett.* 1994. 41: 49–57.

20 Hanninen, A., Maksimow, M., Alam, C., Morgan, D. J. and Jalkanen, S., Ly6C supports preferential homing of central memory $CD8^+$ T cells into lymph nodes. *Eur. J. Immunol.* 2011. 41: 634–644.

21 Walunas, T. L., Bruce, D. S., Dustin, L., Loh, D. Y. and Bluestone, J. A., Ly-6C is a marker of memory $CD8^+$ T cells. *J. Immunol.* 1995. 155: 1873–1883.

22 Bezman, N. A., Kim, C. C., Sun, J. C., Min-Oo, G., Hendricks, D. W., Kamimura, Y., Best, J. A. et al., Molecular definition of the identity and activation of natural killer cells. *Nat. Immunol.* 2012. 13: 1000–1009.

23 Sato, N., Yahata, T., Santa, K., Ohta, A., Ohmi, Y., Habu, S. and Nishimura, T., Functional characterization of NK1.1+Ly-6C+ cells. *Immunol. Lett.* 1996. 54: 5–9.

24 Chiossone, L., Chaix, J., Fuseri, N., Roth, C., Vivier, E. and Walzer, T., Maturation of mouse NK cells is a 4-stage developmental program. *Blood* 2009. 113: 5488–5496.

25 Moretta, A., Poggi, A., Pende, D., Tripodi, G., Orengo, A. M., Pella, N., Augugliaro, R. et al., CD69-mediated pathway of lymphocyte activation: anti-CD69 monoclonal antibodies trigger the cytolytic activity of different lymphoid effector cells with the exception of cytolytic T lymphocytes expressing T cell receptor alpha/beta. *J. Exp. Med.* 1991. 174: 1393–1398.

26 Falco, M., Marcenaro, E., Romeo, E., Bellora, F., Marras, D., Vely, F., Ferracci, G. et al., Homophilic interaction of NTBA, a member of the CD2 molecular family: induction of cytotoxicity and cytokine release in human NK cells. *Eur. J. Immunol.* 2004. 34: 1663–1672.

27 Flaig, R. M., Stark, S. and Watzl, C., Cutting edge: NTB-A activates NK cells via homophilic interaction. *J. Immunol.* 2004. 172: 6524–6527.

28 Nieto, M., Rodriguez-Fernandez, J. L., Navarro, F., Sancho, D., Frade, J. M., Mellado, M., Martinez, A. C. et al., Signaling through CD43 induces natural killer cell activation, chemokine release, and PYK-2 activation. *Blood* 1999. 94: 2767–2777.

29 Andrews, D. M., Scalzo, A. A., Yokoyama, W. M., Smyth, M. J. and Degli-Esposti, M. A., Functional interactions between dendritic cells and NK cells during viral infection. *Nat. Immunol.* 2003. 4: 175–181.

30 Kuribayashi, K., Gillis, S., Kern, D. E. and Henney, C. S., Murine NK cell cultures: effects of interleukin-2 and interferon on cell growth and cytotoxic reactivity. *J. Immunol.* 1981. 126: 2321–2327.

31 Meazza, R., Azzarone, B., Orengo, A. M. and Ferrini, S., Role of common-gamma chain cytokines in NK cell development and function: perspectives for immunotherapy. *J. Biomed. Biotechnol.* 2011. 2011: 861920.

32 Russell, J. H. and Ley, T. J., Lymphocyte-mediated cytotoxicity. *Annu. Rev. Immunol.* 2002. 20: 323–370.

33 **Andrade, F., Roy, S., Nicholson, D., Thornberry, N., Rosen, A. and Casciola-Rosen, L.**, Granzyme B directly and efficiently cleaves several downstream caspase substrates: implications for CTL-induced apoptosis. *Immunity* 1998. **8**: 451–460.

34 **Alter, G., Malenfant, J. M. and Altfeld, M.**, CD107a as a functional marker for the identification of natural killer cell activity. *J. Immunol. Methods* 2004. **294**: 15–22.

35 **Ogasawara, K., Hida, S., Azimi, N., Tagaya, Y., Sato, T., Yokochi-Fukuda, T., Waldmann, T. A. et al.**, Requirement for IRF-1 in the microenvironment supporting development of natural killer cells. *Nature* 1998. **391**: 700–703.

36 **Kennedy, M. K., Glaccum, M., Brown, S. N., Butz, E. A., Viney, J. L., Embers, M., Matsuki, N. et al.**, Reversible defects in natural killer and memory CD8 T cell lineages in interleukin 15-deficient mice. *J. Exp. Med.* 2000. **191**: 771–780.

37 **Zhang, G., Budker, V. and Wolff, J. A.**, High levels of foreign gene expression in hepatocytes after tail vein injections of naked plasmid DNA. *Hum. Gene Ther.* 1999. **10**: 1735–1737.

38 **Zhang, G., Gao, X., Song, Y. K., Vollmer, R., Stolz, D. B., Gasiorowski, J. Z., Dean, D. A., et al.**, Hydroporation as the mechanism of hydrodynamic delivery. *Gene Ther.* 2004. **11**: 675–682.

39 **Inagaki, F. F., Tanaka, M., Inagaki, N. F., Yagai, T., Sato, Y., Sekiguchi, K., Oyaizu, N. et al.**, Nephronectin is upregulated in acute and chronic hepatitis and aggravates liver injury by recruiting CD4 positive cells. *Biochem. Biophys. Res. Commun.* 2013. **430**: 751–756.

40 **Lucas, M., Schachterle, W., Oberle, K., Aichele, P. and Diefenbach, A.**, Dendritic cells prime natural killer cells by trans-presenting interleukin 15. *Immunity* 2007. **26**: 503–517.

41 **Eidenschenk, C., Crozat, K., Krebs, P., Arens, R., Popkin, D., Arnold, C. N., Blasius, A. L. et al.**, Flt3 permits survival during infection by rendering dendritic cells competent to activate NK cells. *Proc. Natl. Acad. Sci. USA* 2010. **107**: 9759–9764.

42 **Stonier, S. W. and Schluns, K. S.**, Trans-presentation: a novel mechanism regulating IL-15 delivery and responses. *Immunol. Lett.* 2010. **127**: 85–92.

43 **Napolitani, G., Rinaldi, A., Bertoni, F., Sallusto, F. and Lanzavecchia, A.**, Selected Toll-like receptor agonist combinations synergistically trigger a T helper type 1-polarizing program in dendritic cells. *Nat. Immunol.* 2005. **6**: 769–776.

44 **Zhu, Q., Egelston, C., Vivekanandhan, A., Uematsu, S., Akira, S., Klinman, D. M., Belyakov, I. M. et al.**, Toll-like receptor ligands synergize through distinct dendritic cell pathways to induce T cell responses: implications for vaccines. *Proc. Natl. Acad. Sci. USA* 2008. **105**: 16260–16265.

45 **Caligiuri, M. A.**, Human natural killer cells. *Blood* 2008. **112**: 461–469.

46 **Kaech, S. M., Tan, J. T., Wherry, E. J., Konieczny, B. T., Surh, C. D. and Ahmed, R.**, Selective expression of the interleukin 7 receptor identifies effector CD8 T cells that give rise to long-lived memory cells. *Nat. Immunol.* 2003. **4**: 1191–1198.

47 **Wherry, E. J. and Ahmed, R.**, Memory CD8 T-cell differentiation during viral infection. *J. Virol.* 2004. **78**: 5535–5545.

48 **O'Leary, J. G., Goodarzi, M., Drayton, D. L. and von Andrian, U. H.**, T cell- and B cell-independent adaptive immunity mediated by natural killer cells. *Nat. Immunol.* 2006. **7**: 507–516.

49 **Sun, J. C., Beilke, J. N. and Lanier, L. L.**, Adaptive immune features of natural killer cells. *Nature* 2009. **457**: 557–561.

50 **Sun, J. C., Beilke, J. N., Bezman, N. A. and Lanier, L. L.**, Homeostatic proliferation generates long-lived natural killer cells that respond against viral infection. *J. Exp. Med.* 2011. **208**: 357–368.

*Full correspondence:* Dr. Yutaka Enomoto, Laboratory of Cell Growth and Differentiation, Institute of Molecular and Cellular Biosciences, The University of Tokyo, 1-1-1 Yayoi, Bunkyo-ku, Tokyo 113-0032, Japan
Fax: +81-3-5841-8475
e-mail: yenomoto@iam.u-tokyo.ac.jp

*Additional correspondence:* Dr. Atsushi Miyajima, Laboratory of Cell Growth and Differentiation, Institute of Molecular and Cellular Biosciences, The University of Tokyo; 1-1-1 Yayoi, Bunkyo-ku, Tokyo 113-0032, Japan
e-mail: miyajima@iam.u-tokyo.ac.jp

Received: 16/2/2014
Revised: 9/6/2014
Accepted: 1/7/2014
Accepted article online: 3/7/2014

 

PLOS | ONE

RESEARCH ARTICLE

# Oncostatin M Maintains the Hematopoietic Microenvironment in the Bone Marrow by Modulating Adipogenesis and Osteogenesis

**Fumi Sato[1], Yuichiro Miyaoka[1¤], Atsushi Miyajima[1], Minoru Tanaka[2,3]***

**1.** Laboratory of Cell Growth and Differentiation, Institute of Molecular and Cellular Biosciences, The University of Tokyo, Tokyo, Japan, **2.** Laboratory of Stem Cell Regulation, Institute of Molecular and Cellular Biosciences, The University of Tokyo, Tokyo, Japan, **3.** Department of Regenerative Medicine, Research Institute, National Center for Global Health and Medicine, Tokyo, Japan

*tanaka@iam.u-tokyo.ac.jp

¤ Current address: Gladstone Institute of Cardiovascular Disease, San Francisco, California, United States of America





**Citation:** Sato F, Miyaoka Y, Miyajima A, Tanaka M (2014) Oncostatin M Maintains the Hematopoietic Microenvironment in the Bone Marrow by Modulating Adipogenesis and Osteogenesis. PLoS ONE 9(12): e116209. doi:10.1371/journal.pone.0116209

**Editor:** Hiroyasu Nakano, Toho University School of Medicine, Japan

**Received:** June 17, 2014

**Accepted:** December 4, 2014

**Published:** December 31, 2014



**Data Availability:** The authors confirm that all data underlying the findings are fully available without restriction. All relevant data are within the paper and its Supporting Information files.

**Funding:** This work was supported by Grants-in-Aid for Scientific Research on Innovative Areas 22118006 from the Japan Society for the Promotion of Science, Japan. The funders had no role in study design, data collection and analysis, decision to publish, or preparation of the manuscript.

**Competing Interests:** The authors have declared that no competing interests exist.

## Abstract

The bone marrow (BM) is an essential organ for hematopoiesis in adult, in which proliferation and differentiation of hematopoietic stem/progenitor cells (HSPC) is orchestrated by various stromal cells. Alterations of BM hematopoietic environment lead to various hematopoietic disorders as exemplified by the linking of fatty marrow with increased adipogenesis to anemia or pancytopenia. Therefore, the composition of mesenchymal stromal cell (MSC)-derived cells in the BM could be crucial for proper hematopoiesis, but the mechanisms underlying the MSC differentiation for hematopoiesis remain poorly understood. In this study, we show that Oncostatin M (OSM) knock out mice exhibited pancytopenia advancing fatty marrow with age. OSM strongly inhibited adipogenesis from BM MSC *in vitro*, whereas it enhanced their osteogenesis but suppressed the terminal differentiation. Intriguingly, OSM allowed the MSC-derived cells to support the *ex vivo* expansion of HSPC effectively as feeder cells. Furthermore, the administration of OSM in lethally irradiated wild-type mice blocked fatty marrow and enhanced the recovery of HSPC number in the BM and peripheral blood cells after engraftment of HSPC. Collectively, OSM plays multiple critical roles in the maintenance and development of the hematopoietic microenvironment in the BM at a steady state as well as after injury.

## Introduction

The bone marrow (BM) is a major tissue that supplies blood throughout life. Hematopoietic stem cells (HSC) are surrounded by various types of stromal cells and the proliferation and differentiation of HSC is tightly regulated in the BM microenvironment [1]. Two types of functional niches for supporting HSC in the BM have been studied; i.e., the osteoblastic niche [2–4] and perivascular niche [5–7], which are composed of osteoblasts and endothelial cells/perivascular mesenchymal cells, respectively. Mesenchymal stromal cells (MSC) in the BM can give rise to multiple cell lineages *in vitro*, including adipocytes, osteocytes, and chondrocytes [8, 9]. Recently, it has been reported that a subset of MSC (PDGFα+Sca-1+CD45-TER119-; PαS cell) in the BM could differentiate into hematopoietic niche cells, osteoblasts, and adipocytes after *in vivo* transplantation [10], although it remains to be elucidated whether the PαS-derived cells function as HSPC niche in the BM and what factors regulate the differentiation of PαS cell *in vivo*.

On the other hand, Naveiras et al. reported the BM adipocytes as negative regulators of the hematopoietic microenvironment using lipoatrophic A-ZIP/F1 'fatless' mice [11]. In the study, transplantation of normal BM cells in lethally irradiated A-ZIP/F1 mice lacking adipogenesis showed enhanced hematopoietic recovery compared with wild-type recipient mice, indicating that adipocytes in fatty marrow hinder hematopoietic progenitor expansion. In humans, it is also known that fatty marrow gradually predominates with age [12]. It should be noted that some myeloid diseases such as aplastic anemia (AA) displaying anemia, and/or pancytopenia are accompanied by severe fatty marrow [13]. These reports strongly suggest that the cellularity of adipocytes, osteoblasts and other mesenchymal stromal cells in the BM is critical for an adequate hematopoietic microenvironment. As these cells could be derived from MSC in the BM, the factor(s) that regulate their balance would be a novel therapeutic target for impaired hematopoiesis in fatty marrow and for enhancing hematopoietic engraftment after BM transplantation.

OSM is a member of the interleukin (IL)-6 family of cytokines and has various unique biological activities e.g. hematopoiesis, hepatogenesis and adipogenesis, which are not shared by the other family members [14]. Murine OSM is expressed in the aorta-gonad-mesonephros (AGM) region, where long-term repopulating HSC (LT-HSC) arise, and OSM stimulates the expansion of multipotential hematopoietic progenitors in the primary culture of AGM [15]. While OSM also expanded hematopoietic stem/progenitor cells (HSPC) in co-cultures of AGM and fetal liver cells [16], it induced the differentiation of fetal hepatocytes *in vitro* [17]. Despite its strong and unique activities *in vitro*, the genetic ablation of either OSM or its receptor (OSMR) in mice unexpectedly showed no severe defects during development [18, 19]. In contrast, these adult knockout (KO) mice displayed anemic and thrombocytopenic phenotype although the symptoms were relatively mild. Colony-forming unit (CFU) assays showed that the number of hematopoietic progenitors in BM was significantly reduced in KO mice compared

to wild-type (WT) mice, whereas that in spleen was increased. Additionally, the number of hematopoietic progenitors in peripheral blood was increased in OSM KO mice, indicating the mobilization of HSPC from the BM into the circulation. These reports suggest the possibility that the BM niche harboring HSPC is impaired in OSM KO mice.

OSM was shown to inhibit the adipocytic differentiation of 3T3L1 cells, a preadipocyte cell line, mouse embryonic fibroblasts (MEFs), adipose tissue-derived MSC and BM MSC [20–22]. Considering the BM adipocytes as a negative regulator of the hematopoietic microenvironment [11], the lack of inhibitory effect of OSM on adipogenesis from MSC may account for the reduced hematopoietic activity in OSM KO BM. However, the causal linkage between these two original findings has remained uninvestigated. Although Walker et al. reported that marrow adipocyte volume was increased in 12-week-old OSMR KO mice [22], the role of OSM in the BM microenvironment for hematopoiesis has not been elucidated. By contrast, several reports have demonstrated that OSM induces osteogenic differentiation of human MSC and a murine stromal cell line [21–23], suggesting a role for OSM in the hematopoietic microenvironment.

In this report, we aimed to unravel the roles of OSM in the BM hematopoietic microenvironment under various conditions, BM injuries by chemicals or irradiation and aging. In addition, we prepared PαS MSC from WT and OSMR KO BM to examine the biological activities of OSM in their adipogenic and osteogenic differentiation and evaluated the hematopoietic capacity by developing a co-culture system with HSPC. We further present the possibility to use OSM as a promising therapeutic agent to enhance the recovery of hematopoiesis after BM lesion. Our results demonstrate that OSM contributes to the maintenance of the hematopoietic microenvironment by balancing multiple steps of differentiation of BM MSC in both steady and injured states.

## Materials and Methods

### Mice

C57BL/6J mice were purchased from Clea Japan, Inc. (Tokyo, Japan). CD45.1 (C57BL/6) congenic mice were also purchased from the RIKEN Research Center. OSM KO mice and OSMR KO mice were generated as described previously [18, 19]. All animals were maintained in a standard Specific-Pathogen Free (SPF) room at our animal facility. All animal experiments were performed according to the guidelines approved by the Institutional Animal Care and Use Committee of the University of Tokyo.

### Surgical and chemical treatment

For splenectomy, the spleen was removed surgically from anesthetized 10-week-old mice after the splenic artery was ligated by 4-0″ suture (Vicryl; Ethicon, Inc., Somerville, NJ, USA). For myeloablation, 10 mg of busulfan (Sigma-Aldrich, St.

Louis, MO, USA) were dissolved in 1 mL of acetone (Wako Chemical Co., Kyoto, Japan), and then 4 mL of sterilized distilled water were added to yield a final concentration of 2 mg/mL. Next, 20 mg/kg of busulfan was administered intraperitoneally three times over a 1-week period. Mice were sacrificed 1 week after the final administration.

## Measurement of hematocrit values and plasma Erythropoietin (EPO) levels

Peripheral blood was placed into heparinized Micro-Hematocrit Capillary tubes (Thermo Fisher Scientific, Waltham, MA, USA) and centrifuged at 3000 rpm for 20 min at room temperature. After determining the hematocrit value, the plasma was collected for measurement of the plasma EPO concentration. The plasma EPO concentration was measured using a mouse EPO ELISA kit as described in the manufacturer's protocol (R&D Systems, Minneapolis, MN, USA).

## Preparation of BM sections

The femurs were excited and immersion-fixed in 10% neutral-buffered formalin, pH 7.0–7.5 (Wako) at 4℃ for 24 h. After washing under gently running water, the femurs were demineralized at 4℃ for 12 days in decalcifying Solution B (0.5 M EDTA, pH 7.4) (Wako). For Oil Red O staining, demineralized femurs were immersed sequentially in 5, 10, 15, and 20% sucrose-phosphate-buffered saline (PBS) for 6 h each. Finally, the femurs were embedded in OCT compound (Sakura Finetek Inc., Torrance, CA, USA) and sliced into 14-μm sections using a cryostat (MICROM HM 525; Thermo Fisher Scientific).

## Isolation of PαS cells from adult mouse BM

PαS cells, which co-expressed PDGFRα and Sca-1, but not CD45 and TER119, were isolated from the bone of WT or OSMR KO mice as described by Morikawa et al. [10]. Briefly, bone marrow was flushed out from femurs and tibias of 8–12 mice using 22- and 23-G needles (Terumo) and the remaining bone was ground with a pestle. Then, the crushed bone fragments were treated with 0.2% collagenase (Sigma) for 30 min at 37℃. Next, after depletion of mature red blood cells using hypotonic lysis buffer (0.38% $NH_4Cl$) for 7 min on ice, the cells were incubated with anti-FcR for 15 min on ice. The cells were then incubated with allophycocyanin (APC)-conjugated rat anti-mouse PDGFRα (APA5; eBioscience, San Diego, CA, USA), fluorescein isothiocyanate (FITC)-conjugated rat anti-mouse Sca-1 (E13-161.7; BD Biosciences, Franklin Lakes, NJ, USA), phycoerythrin (PE)-conjugated rat anti-mouse CD45 (30-F11; BD Biosciences), and PE-conjugated rat anti-mouse TER119 (TER-119; eBioscience). After dead cells were excluded by propidium iodide staining, the $CD45^-$ $TER119^-$ $PDGFR\alpha^+$ $Sca\text{-}1^+$ cells were sorted using a Moflo XDP cell sorter (Beckman-Coulter, Fullerton, CA, USA). MSC were sub-cultured in α-MEM (Invitrogen, Carlsbad, CA, USA)